J. Fluid Mech. (2010), *vol.* 653, *pp.* 57–97.
doi:10.1017/S0022112010000182

Submerged wall jets subjected to injection and suction from the wall

SUBHASISH DEY†, TUSHAR K. NATH AND SUJIT K. BOSE

Department of Civil Engineering, Indian Institute of Technology, Kharagpur 721302, West Bengal, India

(Received 4 August 2009; revised 7 January 2010; accepted 10 January 2010; first published online 27 April 2010)

This paper presents an experimental study on turbulent flow characteristics in submerged plane wall jets subjected to injection (upward seepage) and suction (downward seepage) from the wall. The vertical distributions of time-averaged velocity components, turbulence intensity components and Reynolds shear stress at different horizontal distances are presented. The horizontal distributions of wall shear stress determined from the Reynolds shear stress profiles are also furnished. The flow field exhibits a decay of the jet velocity over a horizontal distance. The wall shear stress and the rate of decay of the jet velocity increase in the presence of injection and decrease with suction. Based on the two-dimensional Reynolds-averaged Navier–Stokes equations of a steady turbulent flow, the velocity and Reynolds shear stress distributions in the fully developed zone subjected to no seepage, injection and suction are theoretically computed. The response of the turbulent flow characteristics to injection and suction is analysed from the point of view of similarity characteristics, growth of the length scale and decay of the velocity and turbulence characteristics scales. The significant observation is that the velocity, Reynolds shear stress and turbulence intensities in the fully developed zone are reasonably similar under both injection and suction on applying the appropriate scaling laws. An analysis of the third-order moments of velocity fluctuations reveals that the inner layer of the jet is associated with the arrival of low-speed fluid streaks causing an effect of retardation. On the other hand, the upper layer of the jet is associated with the arrival of high-speed fluid streaks causing an effect of acceleration. Injection influences the near-wall distributions of the third-order moments by increasing the upward turbulent advection of the streamwise Reynolds normal stress. In contrast, suction influences the near-wall distributions of the third-order moments by increasing the downward turbulent advection of the streamwise Reynolds normal stress. Also, injection and suction change the vertical turbulent flux of the vertical Reynolds normal stress in a similar way. The streamwise turbulent energy flux travels towards the jet origin within the jet layer, while it travels away from the origin within the inner layer of the circulatory flow. The turbulent energy budget suggests that the turbulent and pressure energy diffusions oppose each other, and the turbulent dissipation lags the turbulent production. The quadrant analysis of velocity fluctuations reveals that the inward and outward interactions are the primary contributions to the Reynolds shear stress production in the inner and outer layers of the jet, respectively. However, injection induces feeble ejections in the vicinity of the wall.

† Email address for correspondence: sdey@iitkgp.ac.in

1. Introduction

A submerged plane wall jet is described as a jet of fluid that impinges tangentially (or at an angle) on a solid wall surrounded by the same fluid (stationary or moving) progressing along the wall. By virtue of the initially high momentum, the streamwise velocity in the shear flow of the jet exceeds that in the external stream over a downstream reach (Launder & Rodi 1981). In a submerged wall jet, the flow zone of primary interest is the fully developed zone that exists after the developing zone of jet. The jet is confined to a solid wall on one side and the other side is fluid bounded. The jet layer is overlain by a circulatory flow zone having a strong mixing of fluid with flow reversal as shown in figure 1(*a*) (discussed in § 3.1). A classical wall jet is therefore different from a submerged wall jet due to the semi-infinite extent of the unconfined side. Since the boundary conditions for a submerged wall jet are such that the velocities at the wall and on the separation line are zero, the velocity distribution has a peak within the jet layer. Below the peak velocity (in the inner layer of shear flow), the flow is characterized by a boundary-layer flow and the upper flow zone is structurally similar to a free jet. Therefore, a submerged wall jet that is characterized by a shear flow influenced by the wall and an overlying circulatory flow layer is of the self-similarity type of a shear flow. Note that after Townsend (1956, 1976), the boundary-layer equations could be reduced to ordinary differential equations under certain conditions and the flow for which this occurs is termed a 'self-similar' flow. It refers to the scaling of an individual flow parameter by a single functional representation. The classical wall jet was analysed by Glauert (1956), who obtained the similarity solution of the velocity distribution for laminar flow, but in turbulent flow, he did not get complete similarity. Patel & Newman (1961) and Gartshore (1965) described the self-similarity of plane turbulent wall jets in adverse pressure gradients neglecting wall shear stress, but Irwin (1973) included the effect of wall shear stress afterwards. Because of their unique features, submerged wall jets are often prototypical flows for studying the interaction between a wall-bounded and a fluid-bounded shear flow. For instance, if the water levels were different on two sides of a sluice gate, and if a small opening were created by slightly lifting the sluice gate, the flow within the lower water level would take the form of a submerged wall jet. The turbulent flow characteristics of submerged wall jets are complex in general, and the complexity increases when a submerged wall jet is subjected to seepage flow (injection and suction) through the wall. Submerged hydraulic jumps are usually treated as two-dimensional submerged wall-jet flows (McCorquodale 1986). Long, Steffler & Rajaratnam (1990) experimentally studied the flow characteristics of a submerged jump by using a laser Doppler anemometer (LDA) and found that the flow in the fully developed zone exhibited some degree of similarity. Recently, Dey & Sarkar (2006) analysed the degree of similarity in flow and turbulence characteristics of submerged wall jets due to abrupt changes from smooth to rough walls. In another study, Dey & Sarkar (2008) investigated the effect of sand-pasted rough walls on the turbulence characteristics of submerged jumps. While the measurements of flow to date have greatly advanced our understanding of the characteristics of classical wall and submerged wall jets, the vast majority of these measurements were obtained on smooth and rough walls (Launder & Rodi 1981, 1983; McCorquodale 1986). So our knowledge of turbulence characteristics of submerged wall jets subjected to injection (upward seepage) and suction (downward seepage) from the wall is deficient. Amitay & Cohen (1993, 1997) are the only researchers who have studied the mean flow and the instability of plane laminar wall jets subjected to injection and suction. Moreover, little attention has so far been paid to study of the higher moments of velocity fluctuations,

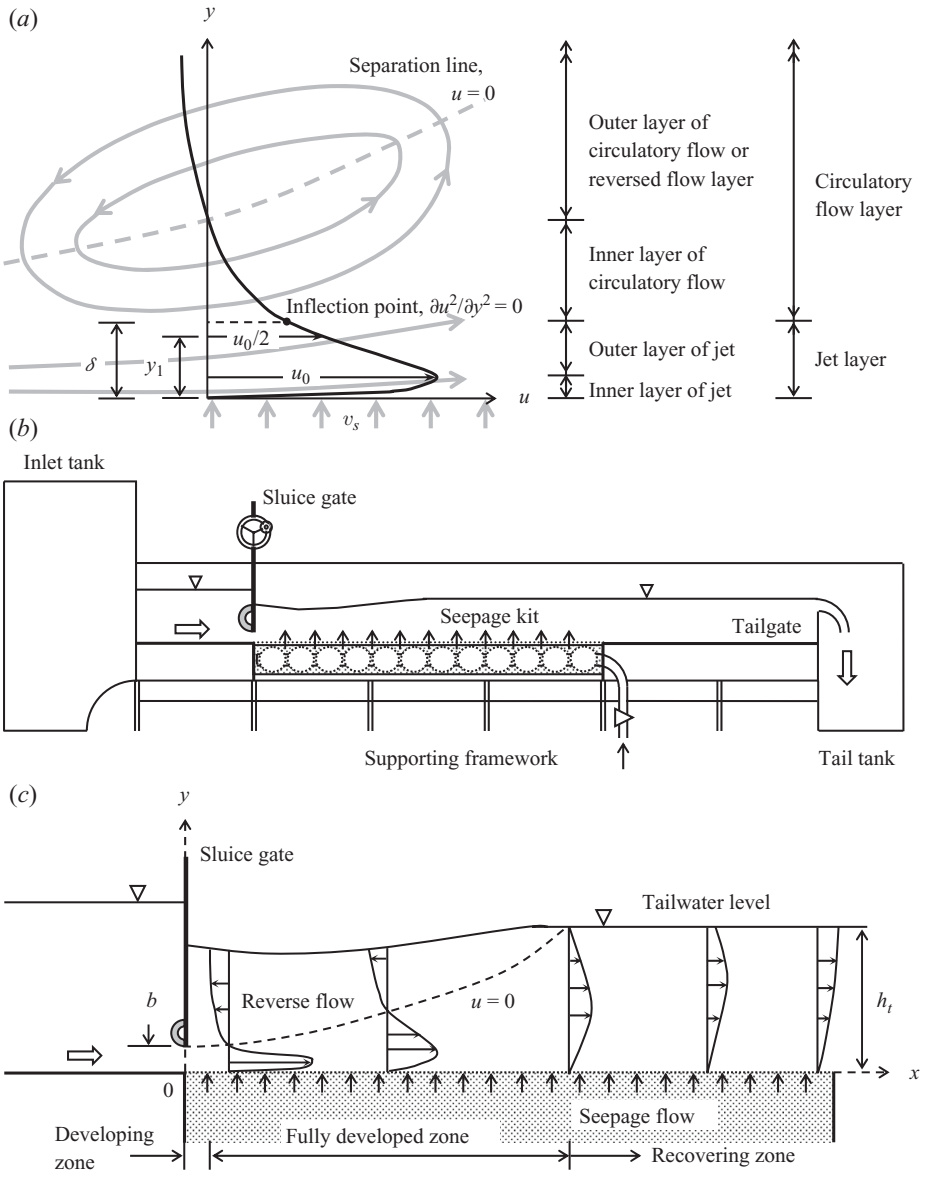

FIGURE 1. (*a*) Typical sketch of the *u*-profile superimposed on the flow field in the fully developed zone; (*b*) schematic of the experimental set-up for a submerged wall jet subjected to injection from the wall; and (*c*) flow zones in a submerged wall jet and the coordinate system. The figure shows the case of injection from the wall; if it were the case of suction, the direction of seepage would be downward.

turbulent energy budget and quadrant analysis of velocity fluctuations in submerged wall jets. The problem is important not only from the viewpoint of the prototypical flows but also in the context of a fundamental study of the response of the turbulent flow characteristics in a submerged wall jet subjected to seepage from the wall. This study therefore aims to investigate the effect of seepage flow (injection and suction)

on the turbulent flow characteristics of submerged wall jets, providing important scaling issues related to the flow and turbulence characteristics and addressing the third-order moments and the quadrant analysis of velocity fluctuations.

Experiments were conducted for submerged wall jets subjected to injection and suction from the wall, having different submergence factors and jet Froude numbers (§ 2). The vertical distributions of time-averaged velocity components, turbulence intensity components and Reynolds shear stress at different streamwise distances were detected by a *Vectrino* velocimeter; and the horizontal distributions of wall shear stress were obtained from the Reynolds shear stress profiles (§ 3). On the basis of the two-dimensional Reynolds-averaged Navier–Stokes (RANS) equations of a steady turbulent flow, the velocity and Reynolds shear stress distributions are theoretically computed (§ 4). The response of the turbulent flow characteristics of submerged wall jets to injection and suction from the wall is analysed from the point of view of similarity, growth of the length scale and decay of the velocity and turbulence characteristics scales (§ 5). Finally, the third-order moments of velocity fluctuations, turbulent energy and contributions of bursting events to Reynolds shear stress production are investigated in detail (§§ 6 and 7).

2. Experimentation

Experiments were carried out in a straight rectangular flume (open channel) that was 0.6 m wide, 0.71 m deep and 12 m long. The sidewalls of the flume were made of transparent glass facilitating visual access. Figure 1(*b*) shows the schematic of the experimental set-up. A Perspex vertical sluice gate that had a smooth curved lip to produce a supercritical wall jet having a thickness equalling the gate opening was fitted over the smooth top-surface of the seepage zone that started from 0.1 m upstream of the gate. Different sluice gate openings $b(= 20–40\,\text{mm})$ were obtained by sliding the gate vertically. The seepage zone that extended downstream of the sluice gate was in the form of a recess known as a seepage kit. It was 0.6 m wide, 0.12 m deep and 2 m long. The casing of the seepage kit was made of Perspex sheets having thickness of 15 mm. Perforated cross-pipes were attached to a main pipe to supply (in the case of injection or upward seepage) water in the kit or to draw out (in the case of suction or downward seepage) from the kit. Four layers of fine filter net with 300 μm opening mesh were placed on the perforated top surface of the seepage kit to achieve a uniform seepage flow. The flow surface formed by the filter net could be considered hydraulically smooth. A valve was fitted to the main pipe to regulate the seepage flow rate ensuring a controlled uniform seepage velocity. The seepage flow rate was measured by an electromagnetic flowmeter. In order to create the desired submergence in the flume, the tailwater depth was controlled by an adjustable tailgate placed at the downstream end of the flume. The free-surface profile was measured by a point gauge with an accuracy of ± 0.1 mm. The discharge at the inlet of the flume controlled by an inlet valve was measured by a calibrated V-notch weir. Altogether 55 sets of measurements were taken, 10 sets on each mode of seepage (injection and suction) and 5 on the no seepage condition. Table 1 provides the important experimental parameters of various runs. The positive and negative values of the seepage velocity v_s refer to injection and suction, respectively. In table 1, the submergence ratio S and jet Froude number F_r are defined as $(h_t - h_j)/h_j$ and $U/(gb)^{0.5}$, respectively. Here, h_t is the tailwater depth, h_j is the conjugate depth of the free jump, U is the issuing jet velocity that is the discharge divided by the area of sluice opening and g is the gravitational acceleration. In this study, h_t was measured at the location of the

b (mm)	U (m s^{-1})	v_s (mm s^{-1})	h_t (m)	S	F_r
20	1.25	0	0.293	3.19	2.82
20	1.25	1	0.295	3.21	2.82
20	1.25	1.5	0.296	3.23	2.82
20	1.25	2	0.298	3.26	2.82
20	1.25	2.5	0.3	3.29	2.82
20	1.25	3	0.302	3.31	2.82
20	1.25	−1	0.291	3.16	2.82
20	1.25	−1.5	0.29	3.14	2.82
20	1.25	−2	0.288	3.11	2.82
20	1.25	−2.5	0.287	3.1	2.82
20	1.25	−3	0.285	3.07	2.82
25	1	0	0.3	4	2.02
25	1	1	0.301	4.02	2.02
25	1	1.5	0.303	4.05	2.02
25	1	2	0.305	4.08	2.02
25	1	2.5	0.307	4.12	2.02
25	1	3	0.308	4.13	2.02
25	1	−1	0.298	3.97	2.02
25	1	−1.5	0.297	3.95	2.02
25	1	−2	0.295	3.92	2.02
25	1	−2.5	0.293	3.88	2.02
25	1	−3	0.292	3.86	2.02
30	0.833	0	0.305	4.88	1.54
30	0.833	1	0.306	4.9	1.54
30	0.833	1.5	0.307	4.92	1.54
30	0.833	2	0.311	5	1.54
30	0.833	2.5	0.313	5.04	1.54
30	0.833	3	0.314	5.06	1.54
30	0.833	−1	0.302	4.83	1.54
30	0.833	−1.5	0.301	4.81	1.54
30	0.833	−2	0.3	4.79	1.54
30	0.833	−2.5	0.299	4.77	1.54
30	0.833	−3	0.298	4.75	1.54
35	0.714	0	0.308	5.84	1.22
35	0.714	1	0.31	5.88	1.22
35	0.714	1.5	0.312	5.93	1.22
35	0.714	2	0.314	5.98	1.22
35	0.714	2.5	0.315	6.02	1.22
35	0.714	3	0.317	6.05	1.22
35	0.714	−1	0.306	5.8	1.22
35	0.714	−1.5	0.304	5.76	1.22
35	0.714	−2	0.302	5.71	1.22
35	0.714	−2.5	0.3	5.67	1.22
35	0.714	−3	0.298	5.62	1.22
40	0.639	0	0.323	6.88	1.02
40	0.639	1	0.325	6.93	1.02
40	0.639	1.5	0.326	6.95	1.02
40	0.639	2	0.327	6.97	1.02
40	0.639	2.5	0.329	7.02	1.02
40	0.639	3	0.331	7.07	1.02
40	0.639	−1	0.321	6.82	1.02
40	0.639	−1.5	0.319	6.78	1.02
40	0.639	−2	0.317	6.73	1.02
40	0.639	−2.5	0.315	6.68	1.02
40	0.639	−3	0.313	6.63	1.02

TABLE 1. Experimental parameters of various runs for different seepage conditions. Note that for the turbulent flow analyses, experiments with $b = 30$ and 40 mm are used, while all experimental data are used to determine length scales.

free-surface profile that became parallel to the flume bottom, and it was calculated as $h_t = 0.5b(\sqrt{1+8F_r^2}-1)$.

A four-beam downlooking acoustic Doppler probe, named *Vectrino*, was used to capture the instantaneous velocity components. It worked with acoustic frequency of 10 MHz having a sampling rate of 100 Hz and adjustable cylindrical sampling volume of 6 mm diameter and 1–9.1 mm height. Although the sampling rate was also adjustable up to 200 Hz, experience showed that the sampling rate of 100 Hz produced least noise in the signal. In the near-wall flow zone, the lowest sampling length of the *Vectrino* measurements was set as 1 mm, and that was increased away from the wall. The closest location to the wall for the measurements was always 2 mm, which ensured that the sampling volume did not touch the wall. On the other hand, in the circulatory flow layer, the sampling length was increased to 4 mm which produced little noise in this layer that had high mixing. Since the measuring location was 5 cm below the probe, the captured data were free from an influence of the *Vectrino* probe. Thus, it provided a semi-non-intrusive measurement with reasonable accuracy. The main advantage of using a *Vectrino* probe was that it is user friendly in comparison to a full-non-intrusive technique like LDV or PIV. However, it made measurement not feasible within the flow zone 5 cm below the free surface, although this zone was not the interest of this study. The finest vertical spacing of the measurements was 2 mm which was maintained within the jet layer. Importantly, the location of the edge of the inner layer of the jet (that is the point of occurrence of the maximum streamwise velocity) and the point of zero velocity (that is the point on the separation line) were determined by fitting smooth curves through the measured velocity plots. In contrast, the closest horizontal spacing of the measurements was 5 cm up to the junction of the fully developed and the recovering zones (figure 1*c*). However, the vertical and horizontal spacing of the measurements were larger in the reversed flow layer and recovering zone, respectively. In order to have a clear presentation avoiding overlapping of profiles or congested data plots, figures representing various characteristics of flow do not always depict all the experimental data at their closest spacing.

The measurements were primarily taken along the vertical lines at different horizontal distances on the centreline of the flume. The two-dimensionality of the flow structure in the central portion of the flume was ascertained by taking some measurements at different transverse locations z (measured from the centreline of the flume) having a fixed horizontal distance, as shown in figure 2(*a*, *b*). An examination of the streamwise velocity u and the Reynolds shear stress $-\rho\overline{u'v'}$ distributions for $v_s = 0$, 3 and $-3\,\mathrm{mm\,s^{-1}}$ reveals that at least in the central portion of the flume (± 0.1 m off the centreline), the flows were reasonably two-dimensional. Here, ρ is the mass density of fluid, u' is the fluctuation of streamwise velocity and v' is the fluctuation of vertical velocity. For the ratio of flume width to flow depth less than 6, the wall-affected zones (wedge shaped) extended from the two sidewalls of a flume start encroaching near the free surface developing a dip in the velocity profiles in a unidirectional open-channel flow (Yang, Tan & Lim 2004). Therefore, in this study, where flume width/flow depth is ≈ 2, the wall-affected zone remained in the circulatory flow layer in the fully developed zone of the jet. Submerged wall jets studied by Long *et al.* (1990), Tachie, Balachandar & Bergstrom (2004) and Dey & Sarkar (2008) with similar width–depth ratios (≈ 2) exhibited a satisfactory two-dimensionality in the central portion of the flume. To ascertain the uniformity in the near-wall velocity and turbulence characteristics under different seepage conditions over a horizontal reach of the seepage kit, additional experiments were conducted for uniform open-channel flows subjected to seepages from the wall. The *Vectrino* measurements were taken

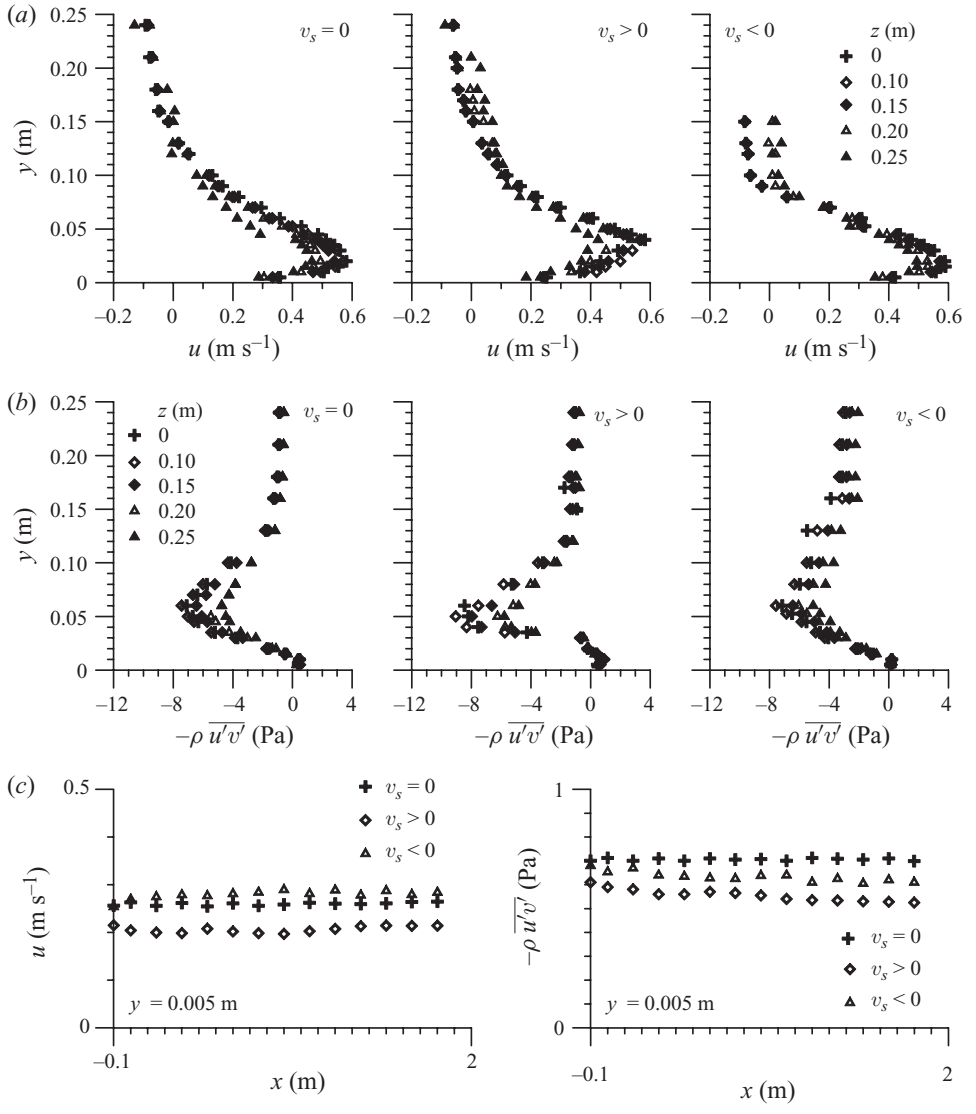

FIGURE 2. (*a*) Plots of u versus y at $x = 0.5$ m (in the fully developed zone) and different z for $U = 0.833$ m s^{-1} and $b = 30$ mm in submerged wall jets subjected to $v_s = 0$, 3 and $v_s = -3$ mm s^{-1}; (*b*) plots of $-\rho\overline{u'v'}$ versus y at $x = 0.5$ m and different z for $U = 0.833$ m s^{-1} and $b = 30$ mm in submerged wall jets subjected to $v_s = 0$, 3 and $v_s = -3$ mm s^{-1}; and (*c*) near-wall ($y = 0.005$ m) horizontal distributions of u and $-\rho\overline{u'v'}$ over the seepage kit in open-channel flows for $v_s = 0$ (with shear velocity $u_\tau = 0.025$ m s^{-1} and flow depth $h = 0.102$ m), $v_s = 3$ mm s^{-1} (with $u_\tau = 0.023$ m s^{-1} and $h = 0.113$ m) and $v_s = -3$ mm s^{-1} (with $u_\tau = 0.029$ m s^{-1} and $h = 0.094$ m).

close to the wall (at a vertical distance, $y = 5$ mm) along the centreline of the flume at different horizontal distances (-0.1 m $\leqslant x \leqslant 1.8$ m). In figure 2(*c*), the horizontal variations of u and $-\rho\overline{u'v'}$ for $v_s = 0, 3$ and -3 mm s^{-1} reveal that a reasonable uniformity in flows prevailed under seepage conditions over the seepage kit, although at the beginning ($x = 0$) of the seepage kit, the flows were not truly uniform under seepage conditions.

v_s (mm s^{-1})	u (cm s^{-1})	v (cm s^{-1})	w (cm s^{-1})	$(\overline{u'u'})^{0.5}$ (cm s^{-1})	$(\overline{v'v'})^{0.5}$ (cm s^{-1})	$(\overline{w'w'})^{0.5}$ (cm s^{-1})	$\overline{u'v'}$ (cm^2 s^{-2})
0	0.382[a]	0.219	0.112	0.109	0.094	0.071	0.867
	(±3.06[b])	(±5.1)	(±3.23)	(±2.56)	(±4.88)	(±1.98)	(±7.12)
3	0.399	0.298	0.145	0.217	0.127	0.099	0.945
	(±4.16)	(±5.56)	(±3.66)	(±3.51)	(±5.14)	(±2.15)	(±7.33)
−3	0.249	0.219	0.101	0.092	0.083	0.049	0.634
	(±2.32)	(±2.87)	(±3.01)	(±2.13)	(±2.99)	(±1.67)	(±4.28)

TABLE 2. Uncertainty estimates of data from *Vectrino* in open-channel flow at $x = 0.6$ m and $y = 5$ mm for different seepage conditions. Note that w is the transverse velocity component and w' is the fluctuation of w. [a]Standard deviation; [b]percentage error.

The adequacy of sampling time was tested by measuring the time-averaged velocity and turbulence quantities using different sampling durations for longer times. Depending on the turbulence intensities, the sampling durations of 180–600 s were found to be adequate in order to have a statistically time-independent averaging. The uncertainty estimates obtained from 15 sets of *Vectrino* data sampled at 100 Hz with a sampling height of 1 mm for a duration of 600 s at $x = 0.6$ m and $y = 5$ mm for different seepage conditions are furnished in table 2. To avoid the bias and random errors of the experimental set-up, every measurement was taken at different times after resuming the experiments. The spectral density functions obtained from the measurements at different locations were found to lie within the 95 % confidence band, confirming the adequacy of 100 Hz sampling frequency for the *Vectrino* measurements.

3. Time-averaged flow field

Figure 1(*c*) schematically illustrates the different flow zones in a submerged wall jet. The flow zones are the 'developing zone' where the submerged wall jet develops in the immediate downstream vicinity of the sluice opening, the 'fully developed zone' where the jet grows up having a circulatory flow on either side of the separation line and the 'recovering zone' that exists downstream of the touching point of the separation line at the free surface. In the recovering zone, the jet flow gradually becomes an open-channel flow, as it flows farther downstream. The time-averaged velocity components in (x, y) are represented by (u, v). The origin of the coordinate axes is located at the junction of the sluice gate and the horizontal wall. Here, x and y are the horizontal and vertical distances, respectively. The flow characteristics are plotted on a non-dimensional $\hat{x}\hat{y}$-plane, where $\hat{x} = x/b$ and $\hat{y} = y/b$. In order to study the influence of the seepage on the turbulent flow field in submerged wall jets, each of figures 3–8 depicts three different runs for $v_s = 0, 3$ and -3 mm s^{-1} having identical jet velocity $U = 0.833$ m s^{-1} and sluice opening $b = 30$ mm. However, all the runs given in table 1 are used to analyse the similarity characteristics of turbulent flow in submerged wall jets.

3.1. *Time-averaged velocity distributions*

Figure 3(*a–c*) represents the vertical distributions of the non-dimensional time-averaged streamwise velocity component $\hat{u}(=u/U)$ at different horizontal distances $\hat{x}$ in submerged wall jets subjected to no seepage ($v_s = 0$), injection ($v_s = 3$ mm s^{-1}) and suction ($v_s = -3$ mm s^{-1}), respectively. In figure 3(*a–c*), the upper and lower lines represent the loci of $u = 0$ (that is the separation line) and $u = u_0$ (that is the

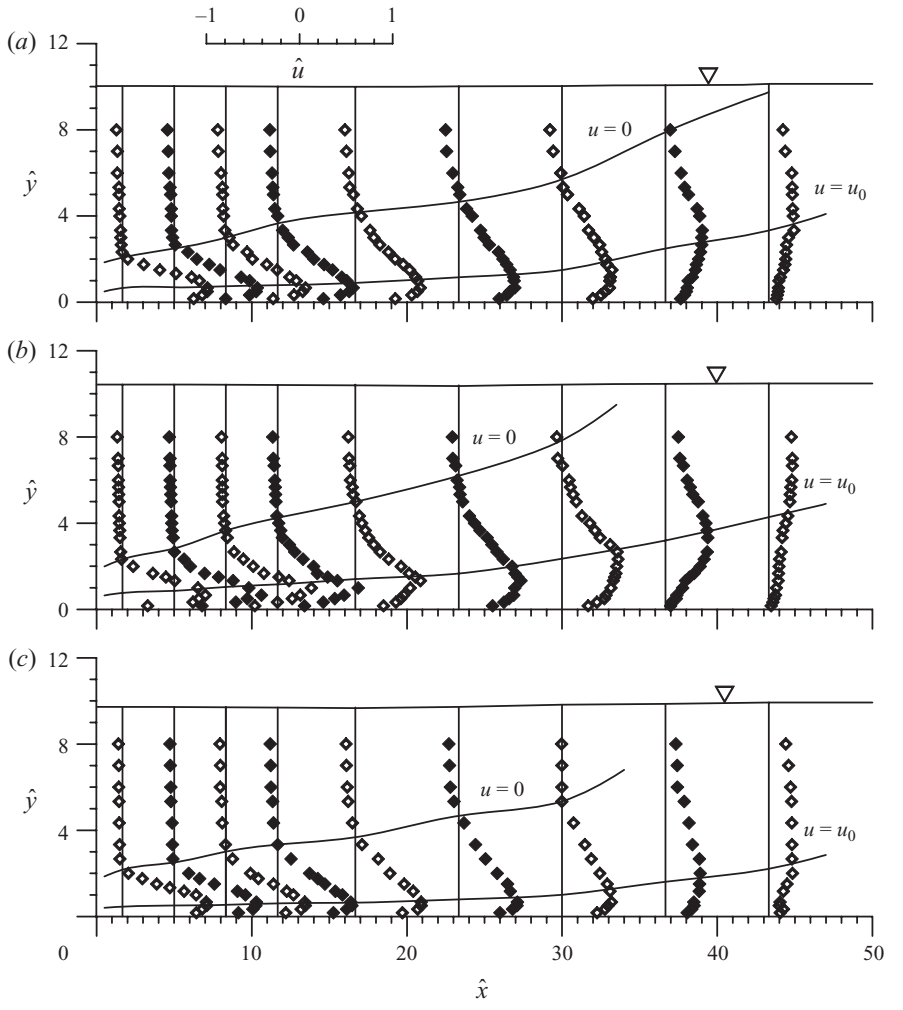

FIGURE 3. Vertical distributions of $\hat{u}$ for $U = 0.833\,\mathrm{m\,s^{-1}}$ and $b = 30\,\mathrm{mm}$ in submerged wall jets subjected to (*a*) $v_s = 0$, (*b*) $v_s = 3\,\mathrm{mm\,s^{-1}}$ and (*c*) $v_s = -3\,\mathrm{mm\,s^{-1}}$.

maximum streamwise velocity of a u-profile) in the submerged wall jets along x. From an examination of the loci of $u = 0$ in figure 3(a, b), it is evident that the length of the fully developed zone where u is a reversal diminishes with an injection from the wall. The loci of $u = u_0$ that show the growth of the inner layer in submerged wall jets become faster in the presence of injection. This phenomenon implies that the decay rate of jet velocity is expedited with an injection. On the other hand, in the case of suction (figure 3*c*), this phenomenon is quite opposite, as the suction delays the decay of jet velocity considerably. Nevertheless, as an inherent characteristic feature of wall jets, the velocity in the jet layer of a submerged wall jet is in general advective decelerating the fluid with horizontal distance. The loci of $u = 0$ touch the free surface at the end of the fully developed zone. Within this zone, a reversal nature of u indicates a strong circulatory flow, whereas in the recovering zone the flow is reasonably horizontal and unidirectional. A typical u-profile in the fully developed zone describing various layers of flow has been shown in figure 1(*a*). The inner and outer layers of the jet refer to the zones below and above the point of occurrence

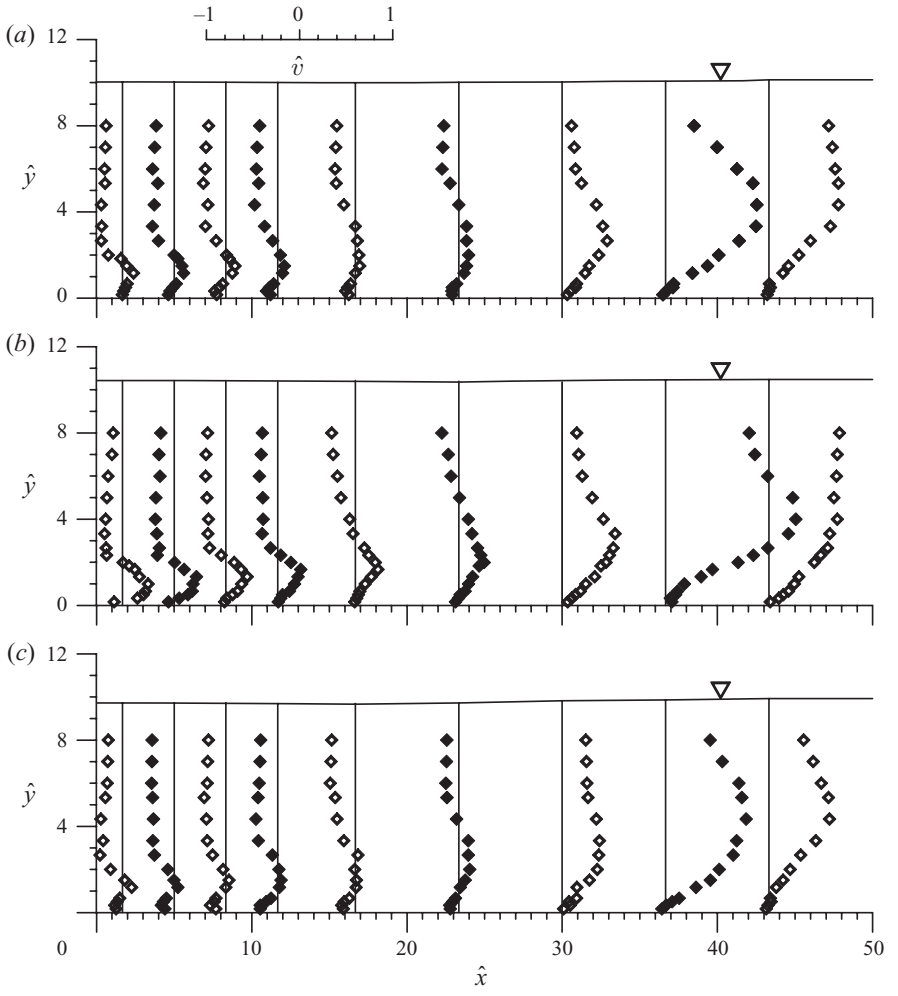

FIGURE 4. Vertical distributions of $\hat{v}$ for $U = 0.833\,\mathrm{m\,s^{-1}}$ and $b = 30\,\mathrm{mm}$ in submerged wall jets subjected to (*a*) $v_s = 0$, (*b*) $v_s = 3\,\mathrm{mm\,s^{-1}}$ and (*c*) $v_s = -3\,\mathrm{mm\,s^{-1}}$.

of u_0. Precisely, the jet layer that comprises inner and outer layers extends up to the inflection point (that is the point of change of slope, $\mathrm{d}u^2/\mathrm{d}y^2 = 0$) of a u-profile. Above the jet layer, there exists a circulatory flow layer that is divided by the separation line $u = 0$ into inner and outer layers of the circulatory flow. The flow in the outer layer of the circulatory flow is directed upstream. Momentum exchange takes place through the separation line within the circulatory flow layer of the jet. The thickness δ of the jet layer and the half-width y_1 of the jet are important from the viewpoint of scaling the distributions of u (§§4 and 5).

The vertical distributions of the non-dimensional time-averaged vertical velocity component $\hat{v}(=v/U)$ at different $\hat{x}$ in submerged wall jets subjected to $v_s = 0$, 3 and $-3\,\mathrm{mm\,s^{-1}}$ are shown in figure 4(*a–c*). Within the jet layer, the upward motion of $\hat{v}$ in the fully developed zone increases in the presence of injection and decreases with suction because of the addition and extraction of momentum through the wall. This phenomenon is also prominent in the recovering zone. However, the change of direction of $\hat{v}$ along the vertical suggests a circulatory flow in the fully developed zone.

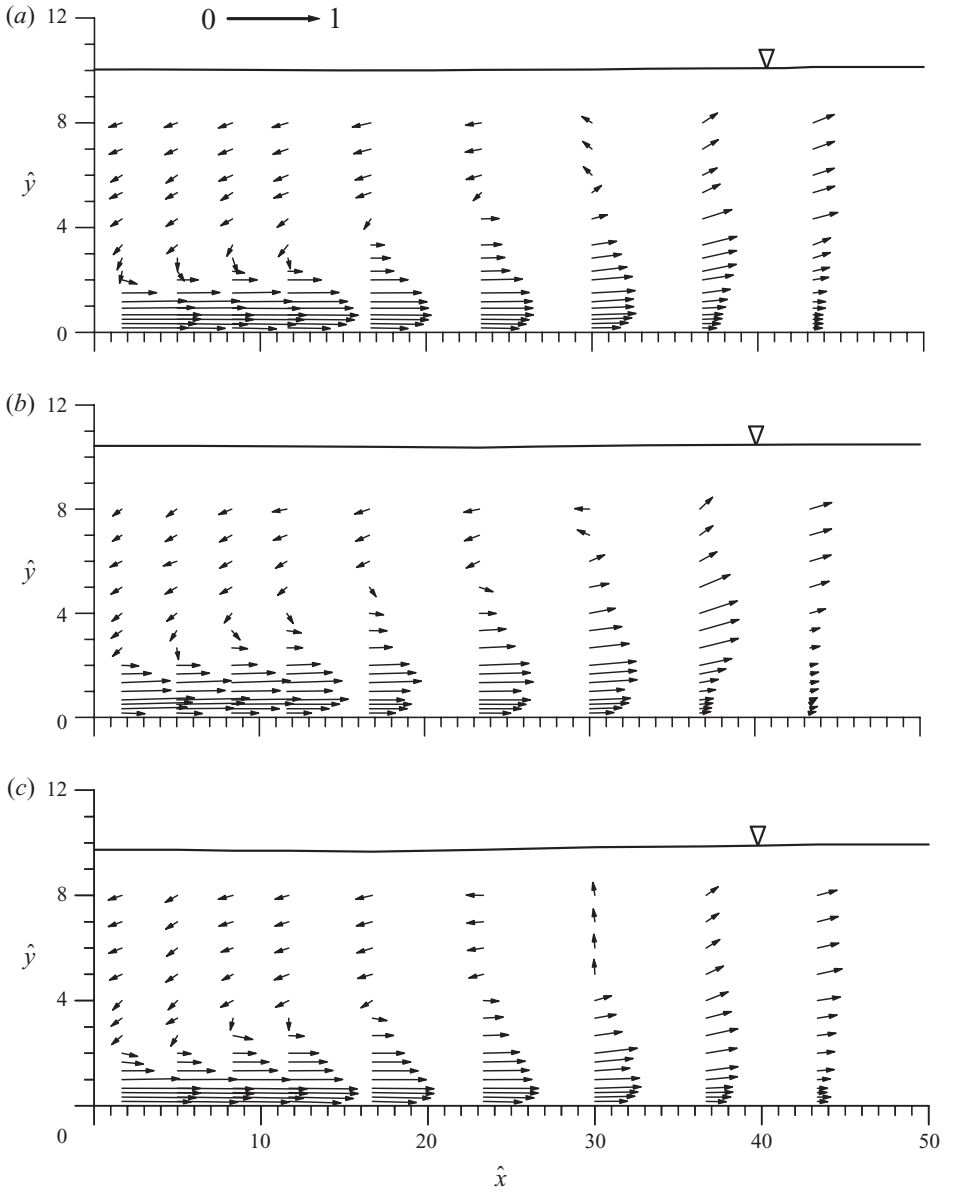

FIGURE 5. Non-dimensional velocity vectors for $U = 0.833\,\mathrm{m\,s^{-1}}$ and $b = 30\,\mathrm{mm}$ in submerged wall jets subjected to (*a*) $v_s = 0$, (*b*) $v_s = 3\,\mathrm{mm\,s^{-1}}$ and (*c*) $v_s = -3\,\mathrm{mm\,s^{-1}}$.

Thus, $\hat{v}$ plays an important role in exchanging the momentum across the separation line.

Figure 5(*a–c*) illustrates the non-dimensional velocity vectors in submerged wall jets subjected to $v_s = 0$, 3 and $-3\,\mathrm{mm\,s^{-1}}$. The characteristics of the decay of the jet and the circulatory flow in the fully developed zone are evident from the magnitude, $(\hat{u}^2 + \hat{v}^2)^{0.5}$, and the direction, $\arctan(\hat{v}/\hat{u})$, of velocity vectors. In addition to the inherent wall jet decay, the reversed flow produces a spatial deceleration that has an influence on the time-averaged flow momentum balance including its structure and the turbulence structure as well. In § 3.2, turbulence structure is discussed in detail.

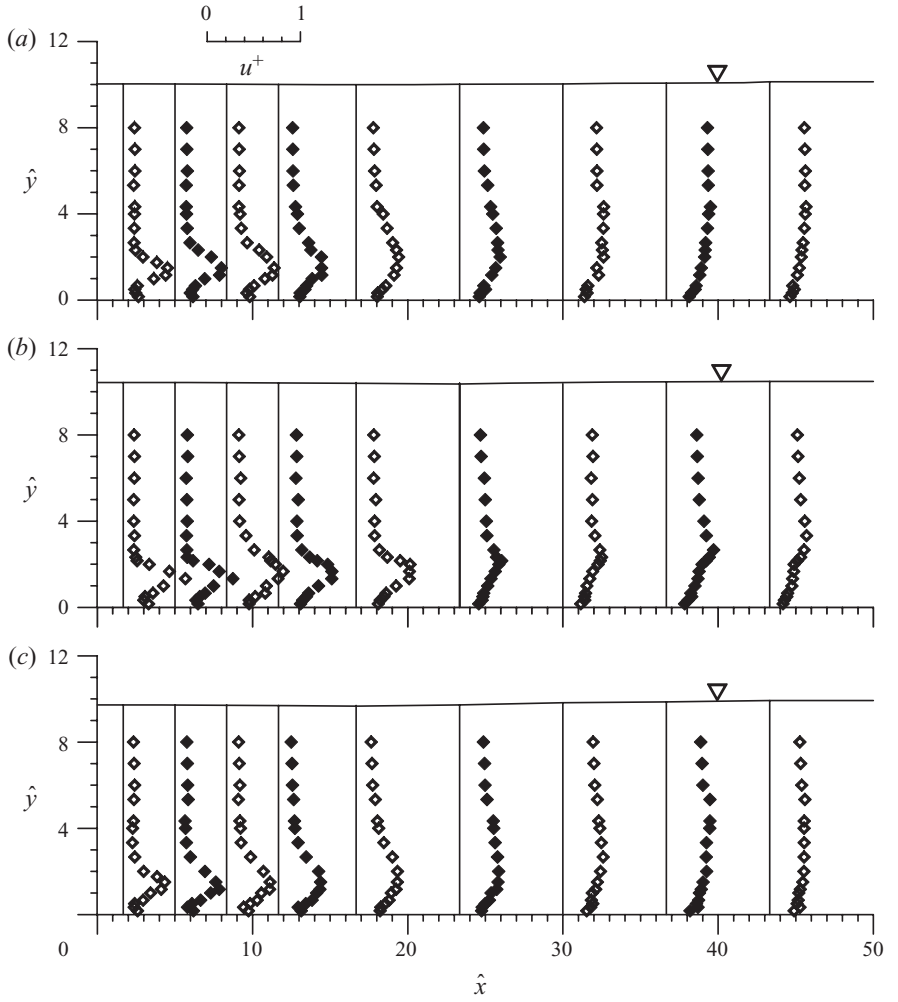

FIGURE 6. Vertical distributions of u^+ for $U = 0.833\,\mathrm{m\,s^{-1}}$ and $b = 30\,\mathrm{mm}$ in submerged wall jets subjected to (*a*) $v_s = 0$, (*b*) $v_s = 3\,\mathrm{mm\,s^{-1}}$ and (*c*) $v_s = -3\,\mathrm{mm\,s^{-1}}$.

3.2. *Turbulence intensities, Reynolds shear stress and wall shear stress distributions*

The vertical distributions of non-dimensional streamwise turbulence intensity $u^+[= (\overline{u'u'})^{0.5}/U]$ at different $\hat{x}$ in submerged wall jets subjected to $v_s = 0$, 3 and $-3\,\mathrm{mm\,s^{-1}}$ are presented in figure 6(*a–c*). In general, the turbulence in the inner layer of the jet is influenced by the overlying reversed flow and its deceleration. An introduction of seepage through the wall makes the turbulence structure more complex. In the developing zone, pronounced protuberances in the distributions of u^+ are evident at the inflection points of u-profiles. The inflection point belongs at the top of the jet layer. The magnitude of u^+ increases because of the circulatory flow over the jet layer. This characteristic is almost absent in the distributions of u^+ in the recovering zone. To be more explicit, the locus of maximum u^+ is advective, receiving turbulent fluid from the jet layer and transporting it towards the circulatory flow layer. The effect of seepage is only noticeable within the jet layer, while the effect is absent within the reversed flow layer, where the distributions of u^+ are almost invariant of the vertical distance. A close examination of the distributions of u^+ reveals that the magnitude

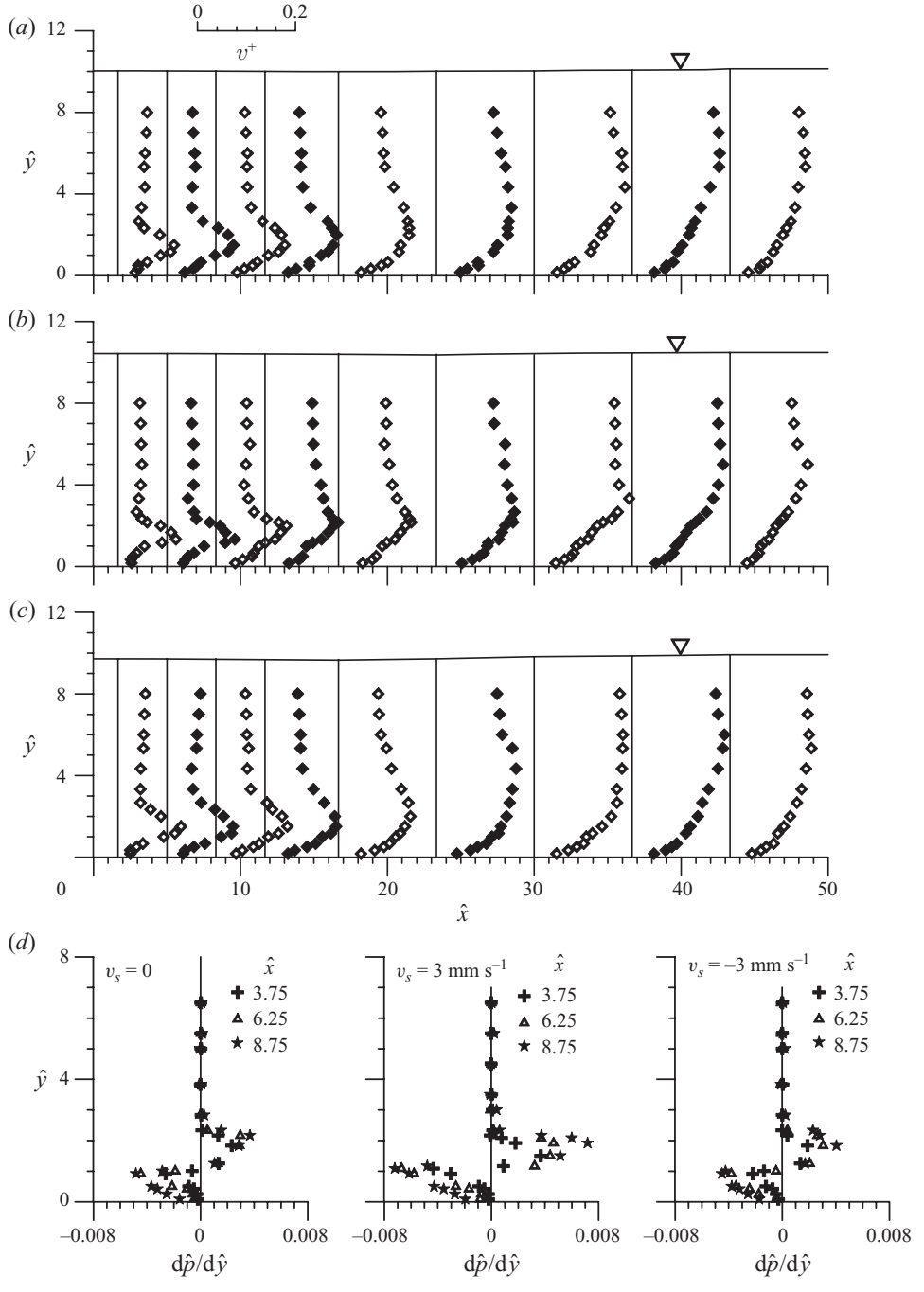

FIGURE 7. Vertical distributions of v^+ for $U = 0.833\,\mathrm{m\,s^{-1}}$ and $b = 30\,\mathrm{mm}$ in submerged wall jets subjected to (*a*) $v_s = 0$, (*b*) $v_s = 3\,\mathrm{mm\,s^{-1}}$, (*c*) $v_s = -3\,\mathrm{mm\,s^{-1}}$; and (*d*) vertical distributions of $d\hat{p}/d\hat{y}$.

of the protuberances increases in the presence of injection and decreases with suction.

Figure 7(*a–c*) shows the vertical distributions of non-dimensional vertical turbulence intensity $v^+[= (\overline{v'v'})^{0.5}/U]$ at different $\hat{x}$ in submerged wall jets subjected to $v_s = 0$,

3 and $-3\,\mathrm{mm\,s^{-1}}$. Protuberances in the distributions of v^+ are also evident near the inflection points of u-profiles. In the fully developed zone, the nature of the distributions of v^+ is quite similar to that of u^+. Although the effect of seepage is not prominent on the distributions of v^+, there is a slight tendency to follow a linear variation of v^+ near the wall in the presence of injection. The large circulatory flow above the jet layer is governed by the pressure gradient which can be related to v^+ in non-dimensional form as $\mathrm{d}\hat{p}/\mathrm{d}\hat{y} = -\mathrm{d}v^{+2}/\mathrm{d}\hat{y}$ (Townsend 1956; Rajaratnam 1976; Dey & Sarkar 2006). Here, $\hat{p}$ is $p/(\rho U^2)$ and p is the piezometric pressure intensity. Figure 7(*d*) presents the non-dimensional pressure gradient $\mathrm{d}\hat{p}/\mathrm{d}\hat{y}$ across the flow layer in submerged wall jets subjected to $v_s = 0$, 3 and $-3\,\mathrm{mm\,s^{-1}}$. In general, $\mathrm{d}\hat{p}/\mathrm{d}\hat{y}$ increases with $\hat{x}$ within the fully developed zone. It is negative in the inner layer of the jet, reaching a negative peak at the point of maximum jet velocity (approximately at $\hat{y} = 1$), and then changes over to positive in the outer layer of the jet, reaching a positive peak at the inflection point of the u-profile. In the circulatory flow layer, $\mathrm{d}\hat{p}/\mathrm{d}\hat{y}$ becomes almost zero. The negative and positive peaks increase in the presence of injection and decrease with suction. The opposing sign of $\mathrm{d}\hat{p}/\mathrm{d}\hat{y}$ governs the circulatory flow.

Figure 8(*a–c*) depicts the vertical distributions of non-dimensional Reynolds shear stress $uv^+ = (-\overline{u'v'}/U^2)$ at different $\hat{x}$ in submerged wall jets subjected to $v_s = 0$, 3 and $-3\,\mathrm{mm\,s^{-1}}$. In the immediate vicinity of the wall, uv^+ is positive within the fully developed zone. It diminishes sharply changing its sign to negative and forming protuberances (maximum negative value of uv^+ in a uv^+-profile) on the line of separation with an increase in the vertical distance $\hat{y}$. These protuberances in the distributions of uv^+ gradually disappear towards the recovering zone, where uv^+ is almost invariant with $\hat{y}$ except within the jet layer. The effect of seepage is noticeable in the distributions of uv^+ within the jet layer subjected to injection, which causes elevation in the location of the null point ($uv^+ = 0$, that is the point of changing sign of uv^+). Figure 8(*d*) illustrates a typical Reynolds shear stress profile in the fully developed zone. Experimental data show that the null point closely corresponds to the point that lies slightly below the occurrence of the maximum u. The point of occurrence of maximum $-\overline{u'v'}$ and the inflection point of the $-\overline{u'v'}$-profile (that is $\mathrm{d}(\overline{u'v'})^2/\mathrm{d}y^2 = 0$) correspond to the inflection point of the u-profile and the point on the separation line, respectively. Interestingly, $-\overline{u'v'}$ does not vanish at the point of $u = u_0$ that occurs approximately at a distance of $0.1b$ above the point of $\overline{u'v'} = 0$, which is in agreement with Irwin (1973). The vertical distance δ_1 of the null point and the half-width y_2 of the $-\overline{u'v'}$-profile are used for scaling in § 5.

The wall shear stress τ_w is estimated from the distributions of uv^+ by extending a mean fitted line, which follows a uv^+-profile (figure 8*d*), on to the wall, as $\tau_w = -\rho\overline{u'v'}|_{y=0}$ (Dey & Sarkar 2006, 2008). Figure 9(*a–c*) shows the distributions of non-dimensional wall shear stress $\hat{\tau}_w [= \tau_w/(\rho U^2)]$ along $\hat{x}$ induced by submerged wall jets subjected to $v_s = 0$, 3 and $-3\,\mathrm{mm\,s^{-1}}$. The wall shear stress $\hat{\tau}_w$ increases with an increase in $\hat{x}$ up to $\hat{x}(= 15\text{–}20)$ reaching a peak, and then decreases with a further increase in $\hat{x}$. In the presence of injection, the magnitude of $\hat{\tau}_w$ decreases by an average 7 % and increases with suction by an average 5 % with respect to $\hat{\tau}_w(v_s = 0)$. The streamwise variation of $\hat{\tau}_w$ is primarily governed by the distributions of uv^+ where the key parameters are $-(\overline{u'v'})_0$ and δ_1 (see figure 8*d*). Here, $-(\overline{u'v'})_0$ refers to the local maximum magnitude in a vertical profile. Importantly, $-(\overline{u'v'})_0$ refers to the protuberance in the uv^+-profiles that change over at an elevation δ_1 contributing to wall shear stress as $\overline{u'v'}|_{y=0}$. Therefore, $\hat{\tau}_w$ is jointly proportional to $-(\overline{u'v'})_0$ and δ_1. In the beginning of the fully developed zone, both $-(\overline{u'v'})_0$ and

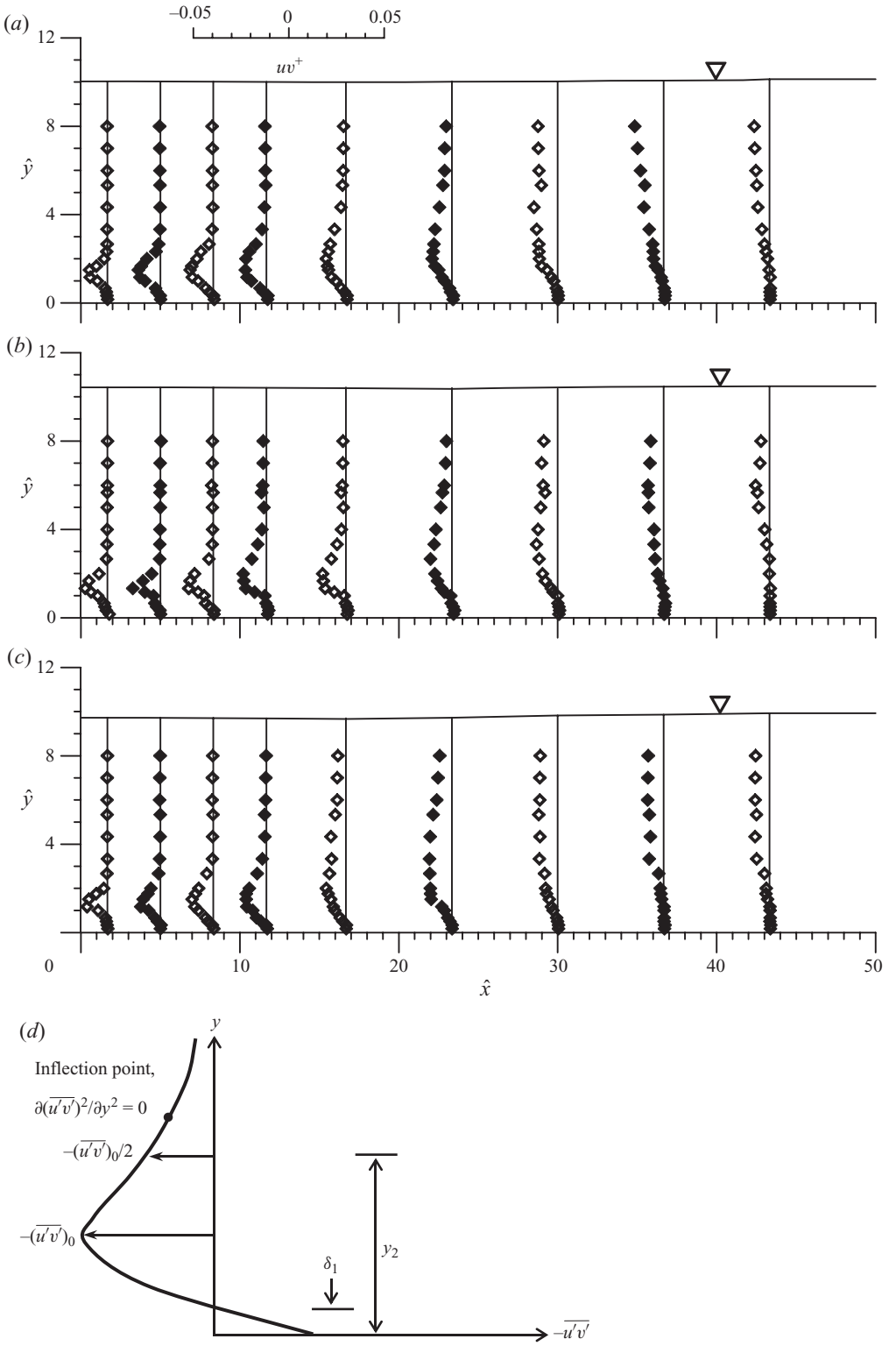

FIGURE 8. Vertical distributions of uv^+ for $U = 0.833\,\mathrm{m\,s^{-1}}$ and $b = 30\,\mathrm{mm}$ in submerged wall jets subjected to (*a*) $v_s = 0$, (*b*) $v_s = 3\,\mathrm{mm\,s^{-1}}$, (*c*) $v_s = -3\,\mathrm{mm\,s^{-1}}$; and (*d*) typical sketch of Reynolds shear stress (relative to ρ) profile in the fully developed zone of a submerged wall jet.

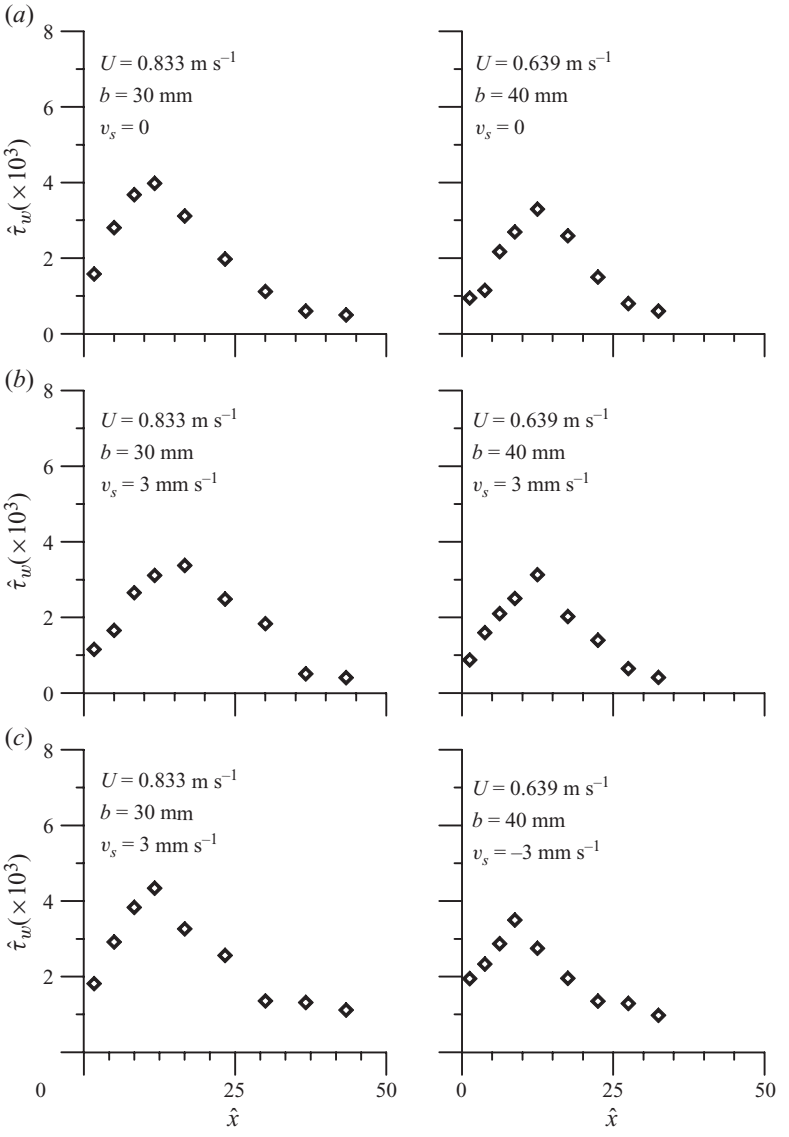

FIGURE 9. Horizontal distributions of $\hat{\tau}_w$ in submerged wall jets subjected to (*a*) $v_s = 0$, (*b*) $v_s = 3\,\text{mm}\,\text{s}^{-1}$ and (*c*) $v_s = -3\,\text{mm}\,\text{s}^{-1}$.

δ_1 are relatively small, but $-(\overline{u'v'})_0$ increases sharply and δ_1 increases slowly with $\hat{x}$ (see figures 15*a* and 17*b* in § 5). Thus, $\hat{\tau}_w$ increases with $\hat{x}$ right away from the sluice gate. The peak of $\hat{\tau}_w$ is associated with the occurrence of maximum $-(\overline{u'v'})_0$ in a uv^+-profile. However, farther downstream, $\hat{\tau}_w$ decreases in accordance with a decrease in $-(\overline{u'v'})_0$, although δ_1 increases slowly and monotonically.

4. Theoretical analysis of flow in submerged wall jets

Figures 1(*a*) and 8(*d*) show typical profiles of u and $-\overline{u'v'}$ in a fully developed zone of a submerged wall jet. We consider a two-dimensional submerged wall jet issuing from a sluice opening subjected to a slow injection (or suction) v_s from the wall, where the jet emerges from the opening as a group of diverging streamlines

and another group of streamlines constituting a circulatory flow above the jet in the circulatory flow zone. The limiting streamline on the wall has velocity $u=0$ due to no-slip. Let the equation of the jet layer be $y=\delta(x_1)$, where $x_1=x+x_0$, up to the point of inflection of the u-profile, assuming the jet layer as a boundary layer. Because of the finite size of the sluice opening, the point of emergence (that is the origin) of the jet is located upstream of the sluice opening at a certain distance x_0. Applying the boundary-layer approximation to the two-dimensional RANS equations of a steady turbulent flow and eliminating the pressure term, the following equation is obtained (Rajaratnam 1976):

$$u\frac{\partial u}{\partial x}+v\frac{\partial u}{\partial y}+\frac{\partial \overline{u'v'}}{\partial y}+\frac{\partial}{\partial x}(\overline{u'u'}-\overline{v'v'})=\upsilon\frac{\partial^2 u}{\partial y^2}, \tag{4.1}$$

where υ is the kinematic viscosity of fluid. The continuity equation is

$$\frac{\partial u}{\partial x}+\frac{\partial v}{\partial y}=0. \tag{4.2}$$

The flow in submerged wall jets is characterized as the self-similar class. To obtain the similarity solutions of (4.1) and (4.2) by the transformation $\eta=y/\delta(x_1)$, where the horizontal length scale x_1 is dimensional for the theory, the solutions are of the form

$$u=u_0\,\varphi(\eta),\quad \overline{u'v'}=-u_0^2\,\psi(\eta)\quad\text{and}\quad \overline{u'u'}-\overline{v'v'}=u_0^2\,\sigma(\eta), \tag{4.3}$$

where $u_0=u_0(x_1)$. Note that a wall jet boundary layer is not amenable to similarity analysis, if different scaling laws are assumed for inner and outer layers of the jet, as was done by e.g. Barenblatt, Chorin & Prostokishin (2005). Inserting the above expressions in (4.1) and using (4.2), one obtains

$$\frac{\delta}{u_0}\frac{\mathrm{d}u_0}{\mathrm{d}x}\varphi^2-\left(\frac{\mathrm{d}\delta}{\mathrm{d}x}+\frac{\delta}{u_0}\frac{\mathrm{d}u_0}{\mathrm{d}x}\right)\varphi'\int_0^\eta\varphi\,\mathrm{d}\eta-\psi'=\frac{1}{R_\delta}\varphi''-\frac{v_s}{u_0}\varphi'-\frac{2\delta}{u_0}\frac{\mathrm{d}u_0}{\mathrm{d}x}\sigma+\frac{\mathrm{d}\delta}{\mathrm{d}x}\sigma'\approx 0, \tag{4.4}$$

where $R_\delta=u_0\delta/\upsilon$. The right-hand side of (4.4) vanishes, as the terms containing v_s and the difference of the streamwise and vertical Reynolds normal stresses represented by σ are negligible and R_δ is large. Since the approximate equation (4.4) does not contain v_s explicitly, it follows that the solution of the equation implicitly depends on v_s. For a similarity solution, (4.4) must be independent of x or x_1 (Schwarz & Cosart 1961), that is

$$\frac{\mathrm{d}\delta}{\mathrm{d}x_1}=\beta\quad\text{and}\quad\frac{\delta}{u_0}\frac{\mathrm{d}u_0}{\mathrm{d}x_1}=-\beta\alpha, \tag{4.5}$$

where β and α are constants. Hence, by integration, one can write

$$\delta=\beta x_1\quad\text{and}\quad u_0=\beta_0 x_1^{-\alpha}, \tag{4.6}$$

where β_0 is a constant. Notably, δ increases linearly with x_1, and u_0 varies as $x_1^{-\alpha}$. In the case of a free jet, α is 0.5 (Schlichting 1979), and so the value of α would deviate from 0.5 depending on the magnitude of v_s.

The velocity distribution obtained from (4.4) and (4.6) is

$$\alpha\varphi^2+(1-\alpha)\varphi'\int_0^\eta\varphi\mathrm{d}\eta+\frac{1}{\beta}\psi'=0. \tag{4.7}$$

Setting $\varphi(\eta)=f'(\eta)$, one obtains the differential equation as

$$\alpha f'^2+(1-\alpha)ff''+\frac{1}{\beta}\psi'=0. \tag{4.8}$$

Introducing turbulence diffusivity ε_f, one can write by definition

$$\overline{u'v'} = -\varepsilon_f \frac{\partial u}{\partial y} = -u_0^2 \psi. \tag{4.9}$$

Using (4.3), (4.9) yields

$$\psi = \frac{\varepsilon_f}{u_0^2}\frac{\partial}{\partial y}(u_0\varphi) = \frac{\varepsilon_f}{u_0\delta}\varphi' = \frac{\varepsilon_f}{\beta_0\beta}\frac{\varphi'}{x_1^{1-\alpha}} = \frac{\varepsilon_0}{\beta_0\beta} f''. \tag{4.10}$$

In (4.10), the left-hand side being independent of x_1 implies that ε_f is proportional to $x_1^{1-\alpha}$, and hence $\varepsilon_f = \varepsilon_0 x_1^{1-\alpha}$. In the narrow turbulent jet layer, ε_0 may be assumed to be an averaged value over η or a constant. Thus, one obtains

$$\alpha f'^2 + (1-\alpha) f f'' + \frac{\varepsilon_0}{\beta_0 \beta^2} f''' = 0. \tag{4.11}$$

The velocity profile contains an arbitrary constant β_0. Replacing β_0 by $4\varepsilon_0/\beta^2$ in (4.11), one gets the following equation for f:

$$\alpha f'^2 + (1-\alpha) f f'' + \frac{1}{4} f''' = 0. \tag{4.12}$$

4.1. *Velocity and Reynolds shear stress distributions*

The boundary conditions applicable for the solution of (4.12) are that at the peak velocity of the jet: $\eta = \eta_0$, $f'(\eta_0) = \varphi(\eta_0) = 1$, $f(\eta_0) = 0$ (that is $v = 0$) and as $\eta \to \infty$, $f'(\eta) = 0$ (that is $u = 0$). For a free jet, $\eta_0 = 0$ and $\alpha = 0.5$ (Schlichting 1979), and the solution of (4.12) is $f = \tanh\eta$. It is anticipated that due to the seepage (and also submergence to some extent), α is modified as

$$\alpha = 0.5 + \alpha_1, \tag{4.13}$$

where α_1 is an additional term mainly due to seepage. The solution of (4.12) can be given by

$$f(\eta) = \tanh(\eta - \eta_0) + \alpha_1 G(\eta). \tag{4.14}$$

Substituting (4.14) in (4.12) and equating the coefficients of α_1, one obtains the differential equation for G as

$$G''' + 2\tanh(\eta-\eta_0)G'' + 4\,\mathrm{sech}^2(\eta-\eta_0)[G' - \tanh(\eta-\eta_0)G + \tanh^2(\eta-\eta_0) + 1] = 0 \tag{4.15}$$

with boundary conditions $G(\eta_0) = 0$, $G'(\eta_0) = 0$ and $G'(\infty) = 0$. Equation (4.15) is a linear differential equation with highly nonlinear coefficients. One can obtain an approximate analytical solution by Galerkin's method. For this purpose, it is recognized that a function of the pattern of the leading term of (4.14) that satisfies the boundary condition is

$$G(\eta) = a_0 \tanh^2(\eta - \eta_0). \tag{4.16}$$

Substituting (4.16) in (4.15) and taking the weighted average with the weight appearing in the equation, one gets

$$a_0 \int_0^\infty \mathrm{sech}^2\eta\ \tanh^3\eta\ (5 - 9\tanh^2\eta)\,\mathrm{d}\eta \approx -\int_0^\infty \mathrm{sech}^2\eta\ \tanh^2\eta\ (1 + \tanh^2\eta)\,\mathrm{d}\eta. \tag{4.17}$$

Numerically evaluating the two integrals in (4.17), one obtains $a_0 \approx 32/15$. Differentiating (4.14) with the value of a_0 obtained in (4.16), one gets

$$\varphi(\eta) = \operatorname{sech}^2(\eta - \eta_0)\left[1 + \frac{64}{15}\alpha_1 \tanh(\eta - \eta_0)\right]. \tag{4.18}$$

Giving the velocity distribution of a submerged wall jet by (4.3) and (4.6), the profile holds for $\eta \geqslant \eta_0$, because below the point of η_0 (that is within the inner layer of the jet), wall effect comes into play.

In the near-wall zone (that is within the inner layer of the jet) $0 < \eta \leqslant \eta_0$, the $1/m$th power law for $\varphi(\eta)$ can be assumed as in the case of flow over a wall. Noting that $\varphi(\eta_0) = 1$, $\varphi'(\eta_0) = 0$, such a law is

$$\varphi(\eta) = \frac{1}{m}\left(\frac{\eta}{\eta_0}\right)^{1/m}\left(1 + m - \frac{\eta}{\eta_0}\right). \tag{4.19}$$

The Reynolds shear stress relative to ρ is given by (4.9) and (4.10) as

$$-\overline{u'v'} = \frac{\beta_0 \varepsilon_0}{\beta} x_1^{-2\alpha} \varphi'(\eta). \tag{4.20}$$

In non-dimensional form, the Reynolds shear stress uv^+ is given by

$$uv^+ = \Theta\,(\hat{x} + \hat{x}_0)^{-2\alpha} \varphi'(\eta), \tag{4.21}$$

where $\Theta = \beta_0 \varepsilon_0/(\beta U^2 b^{2\alpha})$ and $\hat{x}_0 = x_0/b$.

From (4.18) and (4.19), the following expressions for φ' are obtained:

$$\varphi'(\eta \geqslant \eta_0) = -\operatorname{sech}^2(\eta - \eta_0)\left\{2\tanh(\eta - \eta_0) + \frac{64}{15}\alpha_1[2\tanh^2(\eta - \eta_0) - 1]\right\}, \tag{4.22a}$$

$$\varphi'(0 < \eta \leqslant \eta_0) = \frac{1}{m\eta_0}\left(1 + \frac{1}{m}\right)\left(\frac{\eta}{\eta_0}\right)^{(1/m)-1}\left(1 - \frac{\eta}{\eta_0}\right). \tag{4.22b}$$

In (4.22*b*), the Reynolds shear stress vanishes on the wall. Thus, for the computation of wall shear stress, (4.22*b*) cannot be applicable to the wall, where viscous stress prevails within the viscous sublayer. Close to the wall, a very thin layer of a viscous sublayer overlain by a transitional layer merges with the turbulent jet. Assuming a smooth transition between the layers, it is possible to show, as in Bose & Dey (2007) for free surface flows subject to injection, that the non-dimensional streamwise velocity u/u_τ can be expressed as a fifth degree polynomial (truncated Taylor series) in terms of non-dimensional height yu_τ/υ, where u_τ is the shear velocity. In the polynomial, the quadratic term is absent and the coefficient of the cubic term is negligibly small. The expression for the non-dimensional Reynolds shear stress is a polynomial containing a cubic and a quartic term of yu_τ/υ.

4.2. *Determination of constants*

The principal constants requiring estimation from the experimental data are the exponent α and the non-dimensional height η_0 where the maximum velocity u_0 occurs. For the estimation of α_1, first of all, the jet thickness $\delta(x_1)$ is determined by plotting the experimentally observed u at different depths y and x. Using these data, a cubic curve is fitted for the curve $u = u(x, y)$. The zero value of the second derivative ($\mathrm{d}^2u/\mathrm{d}y^2 = 0$) yields the point of inflection, determining the height δ at a distance x. To calculate δ at different x_1, a linear fit to the data $\delta = \beta x_1$ yields the values of $x_0 (= x_1 - x)$ and β. Hence, from (4.3) and $u_0 = \beta_0 x_1^{-\alpha}$, since $\max[\varphi(\eta)] = 1$,

v_s (mm s^{-1})	$\hat{x}_0$	β	β_1	α	α_1	η_0	m	Θ
0	11.34	0.078	3.17	0.455	−0.045	0.3	6	79.87
1	10.01	0.101	3.07	0.446	−0.054	0.35	5	56.52
2	8.38	0.107	2.9	0.438	−0.062	0.4	4	47.71
3	6.97	0.117	2.57	0.426	−0.074	0.42	3	39.74
−1	15.33	0.06	11.25	0.853	0.353	0.22	6.5	2.08×10^4
−2	19.58	0.045	20.37	0.971	0.471	0.2	7	5.55×10^4
−3	23.06	0.044	19.45	0.983	0.483	0.12	7.8	7.14×10^4

TABLE 3. Parameters estimated for different seepage conditions.

$\ln u_0 = \ln\beta_0 - \alpha\ln(x + x_0)$. Thus, fitting a linear equation to the experimental data for u_0 and the estimated values of $(x + x_0)$, one obtains the estimates of α and β_0. As β_0 is dimensional, a non-dimensional parameter $\beta_1 = \beta_0/(Ub^\alpha)$ is taken. Similarly, x_0 is expressed in non-dimensional form as $\hat{x}_0$. As anticipated earlier, α is close to 0.5 yielding the correction α_1 for the submerged wall jets (see (4.13)) subjected to no lateral flow and injection with negative values, while the values of α_1 for suction are slightly higher and turn out to be positive. For no lateral flow, injection and suction, the corresponding estimates of the parameters are given in table 3. Interestingly, the estimation of $\hat{x}_0(v_s = 0)$ obtained by Schwarz & Cosart (1961) for classical wall jets was 11.2, which compares well with the present findings for submerged wall jets with $\hat{x}_0(v_s = 0) = 11.34$. However, the influence of injection and suction on the position of the jet origin is apparent, as injection and suction shift the origin towards and away from the jet origin with no lateral flow, respectively.

The experimental data of streamwise velocity $u/u_0(= \varphi)$ corresponding to η are used to calibrate (4.19) using η_0 and m as free parameters. Table 3 provides the estimated values of η_0 and m. The values of exponent m increase with an increase in suction and decrease with injection. On the other hand, the values of η_0 have a reverse trend to those of m. For the no lateral flow, $m = 6$ corresponds closely with $m = 7$–10 reported by Schlichting (1979) and Dey (2002) for turbulent boundary layer flow over a smooth wall. In the fully developed zone for various $\hat{x}$, figure 10(a, b) shows the collapse of the experimental data on the computed curves obtained from (4.19) for injection and suction, respectively. The effect of negative correction α_1 for the cases of no lateral flow and injection pulls the curves $\varphi = \varphi(\eta > \eta_0)$ down from the curves with $\alpha_1 = 0$. In contrast, for the case of suction, the positive values of α_1 push the curves up from those with $\alpha_1 = 0$.

The experimental data of $-\overline{u'v'}$ corresponding to η are used to calibrate (4.21) computing φ' from (4.22a) and (4.22b) making Θ a free parameter. The estimated values of Θ that increase with an increase in suction and decrease with injection are given in table 3. Figure 11(a, b) shows that the experimental data collapse well on the computed curves $\varphi' = \varphi'(\eta)$ obtained from (4.22a) and (4.22b) for different cases of lateral flows.

5. Similarity characteristics of velocity, Reynolds shear stress and turbulence intensities

5.1. *Length scale*

In submerged wall jets on smooth and rough walls, a horizontal length scale λ for the local maximum jet velocity u_0 is customarily used to collapse all the major

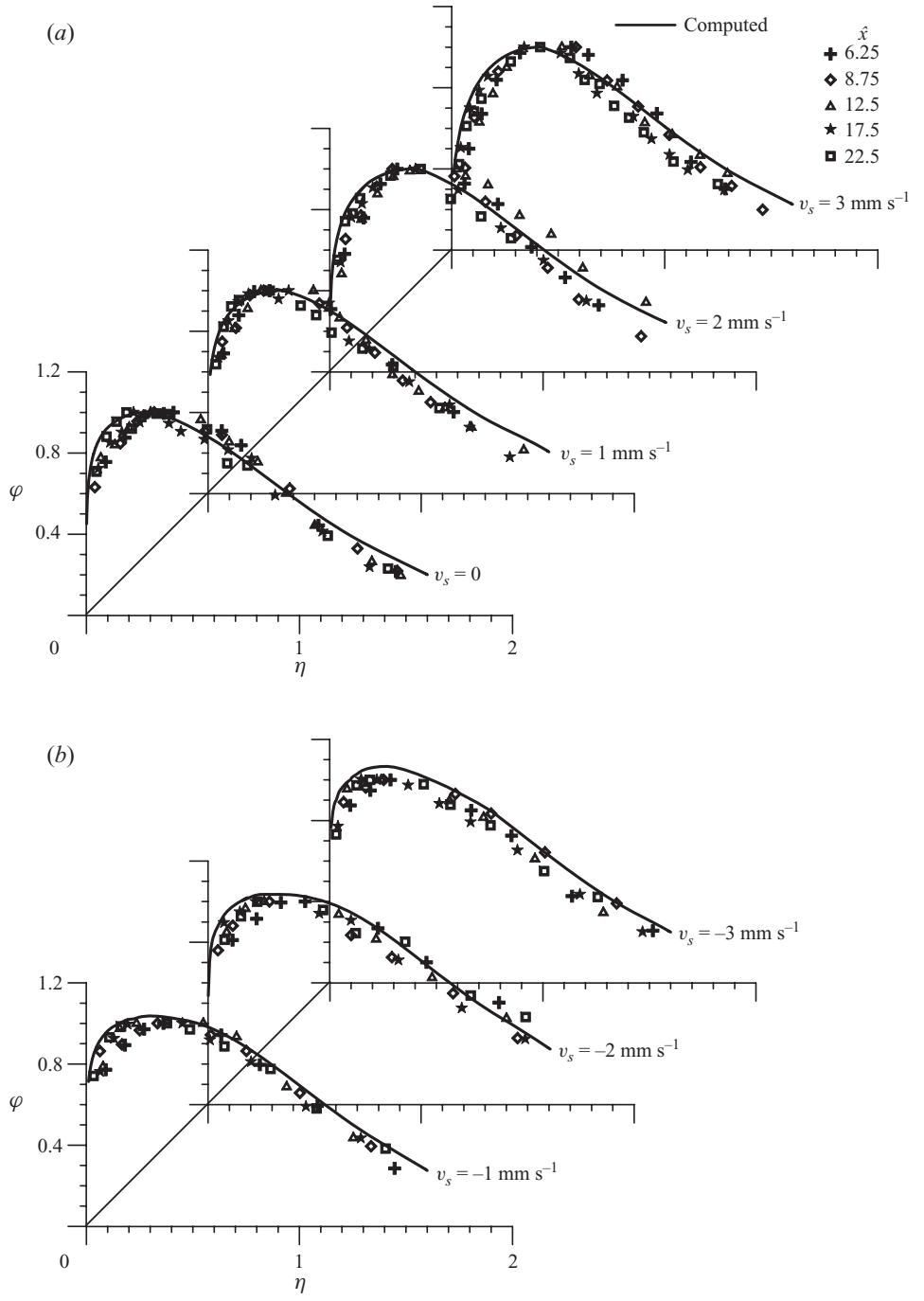

FIGURE 10. φ as a function of η for $U = 0.639\,\mathrm{m\,s^{-1}}$ and $b = 40\,\mathrm{mm}$ in submerged wall jets subjected to different v_s: (*a*) $v_s = 0$, 1, 2 and $3\,\mathrm{mm\,s^{-1}}$ and (*d*) $v_s = -1$, -2 and $-3\,\mathrm{mm\,s^{-1}}$.

velocity or turbulence data on a single band (Long *et al.* 1990; Dey & Sarkar 2006, 2008). The length scale λ is the distance x where $u_0 = U/2$. Narasimha, Narayan & Parthasarathy (1973) and Wygnanski, Katz & Horev (1992) proposed the use of υ and exit momentum $M_0 (= U^2 b)$ to scale u_0 for wall jets. Also, in a couple of previous

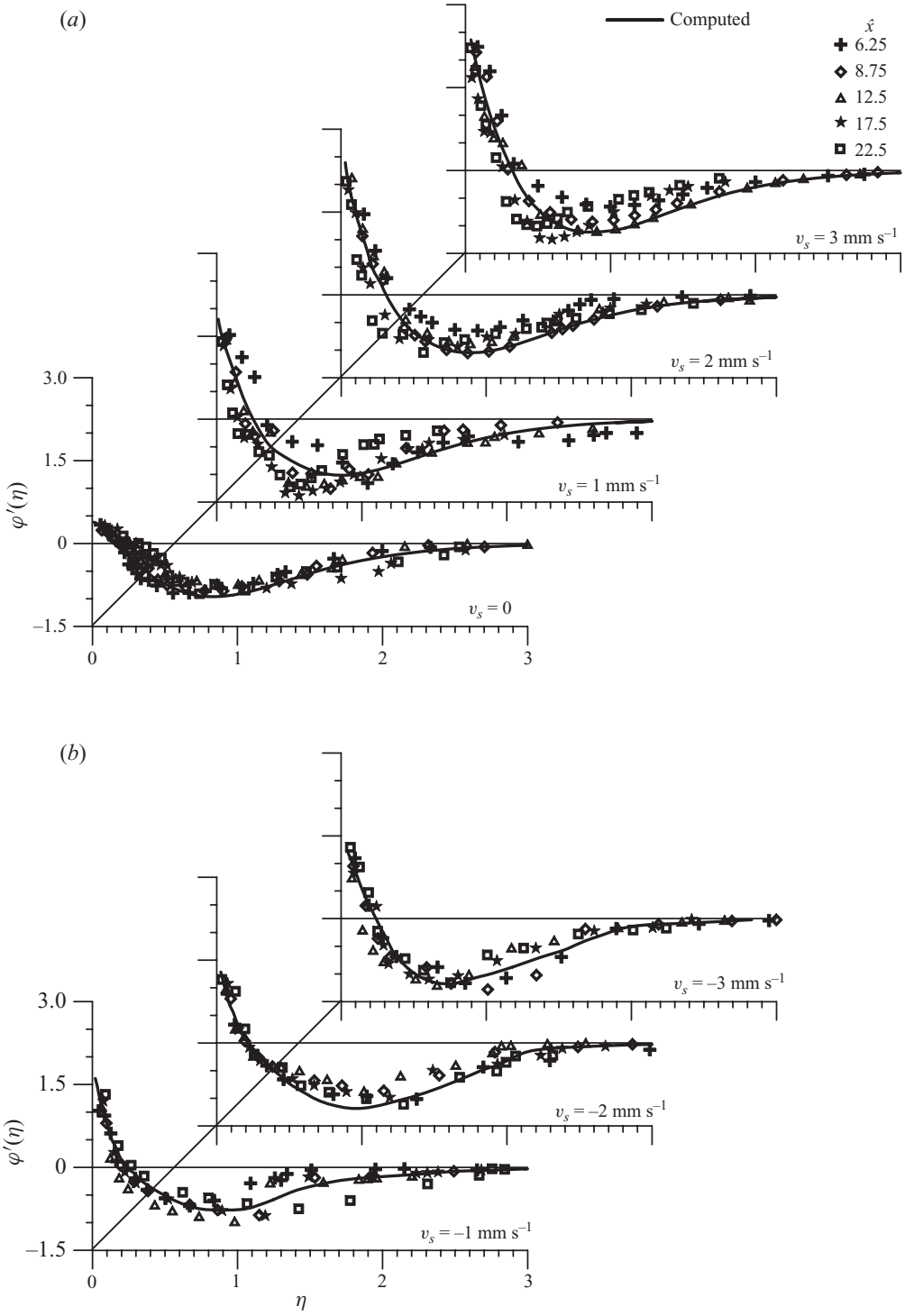

FIGURE 11. $\varphi'(\eta)$ as a function of η for $U = 0.639\,\mathrm{m\,s^{-1}}$ and $b = 40\,\mathrm{mm}$ in submerged wall jets subjected to different v_s: (*a*) $v_s = 0, 1, 2$ and $3\,\mathrm{mm\,s^{-1}}$ and (*b*) $v_s = -1, -2$ and $-3\,\mathrm{mm\,s^{-1}}$.

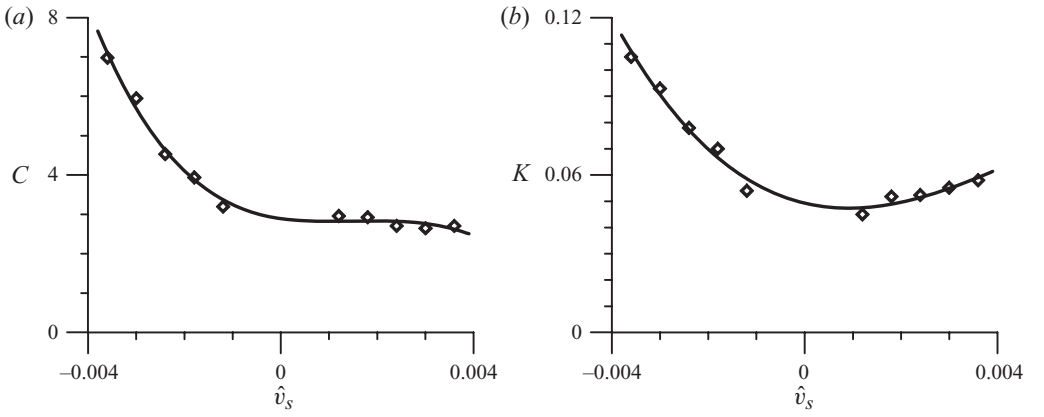

FIGURE 12. Variations of (*a*) C with $\hat{v}_s$ and (*b*) K with $\hat{v}_s$ for submerged wall jets.

studies, sluice opening b was used to scale u_0. However, the scale λ is a superior alternative to use of M_0 or b, as the use of λ could bring down the data to a slim band. Another important aspect is that in the case of a submerged wall jet, the scale should be a function of the submergence S. For a smooth wall, Long *et al.* (1990) proposed the following relationship of λ:

$$\frac{\lambda}{b} = \frac{49}{1 + C_1(\mathrm{d}h/\mathrm{d}x)_\lambda F_r^{-2}}, \tag{5.1}$$

where C_1 is a coefficient and h is the local flow depth. It was argued that the submergence ratio S influences the free surface slope $(\mathrm{d}h/\mathrm{d}x)_\lambda$ at $x = \lambda$. However, to study the submerged wall jets subjected to seepage flows through the wall, $(\mathrm{d}h/\mathrm{d}x)_\lambda$ is a function of S and v_s. Using the least-square curve fitting, one can get the following relationship for different seepage velocities v_s:

$$(\mathrm{d}h/\mathrm{d}x)_\lambda = C_2 \times 10^{-KS}, \tag{5.2}$$

where C_2 and K are the coefficient and exponent, respectively. They vary with v_s. Inserting (5.2) into (5.1), one obtains

$$\frac{\lambda}{b} = \frac{49}{1 + C \times 10^{-KS} F_r^{-2}}, \tag{5.3}$$

where $C = C_1 \times C_2$. The values of C for different non-dimensional seepage velocities $\hat{v}_s (= v_s/U)$ are estimated from the least-square curve fitting of the data plots of λ/b versus $10^{-KS}F_r^{-2}$. The variations of C and K with $\hat{v}_s$ are given in figure 12(*a*, *b*) for injection and suction, respectively.

Alternatively, to scale the individual distributions of velocity and turbulence parameters, various vertical length scales are used. For instance, the length scale y_1 is used for the u-profile (figure 1*a*). It is the distance $y = y_1$, where $u = u_0/2$ and $\partial u/\partial y < 0$, termed 'half-width of jet'. Another length scale y_2 is used for the $-\overline{u'v'}$-profile (figure 8*d*). It is the distance $y = y_2$, where $\overline{u'v'} = (\overline{u'v'})_0/2$ and $\partial(\overline{u'v'})/\partial y < 0$, termed 'half-width of Reynolds shear stress'. Here, the subscript '0' denotes a local peak in a vertical distribution. Besides, the null point of the $-\overline{u'v'}$-profile that occurs at $y = \delta_1$, where $\overline{u'v'} = 0$ and $\partial(\overline{u'v'})/\partial y > 0$, is also used.

5.2. *Similarity characteristics of velocity*

The plots for data sets having sluice openings $b = 30$ and 40 mm used to represent the decay of maximum velocity u_0, in the fully developed zone, over x in submerged wall jets subjected to injection and suction from the wall are shown in figure 13(*a*). The use of the horizontal length scale λ for representing non-dimensional horizontal distance $\tilde{x}(= x/\lambda)$ makes it possible for all the u_0/U data to collapse on a single band, revealing that the similarity characteristic of submerged wall jets under seepage flows exists. The curves of a classical wall jet (Rajaratnam 1976), a free jump (Rajaratnam 1965) and a submerged wall jet (Long *et al.* 1990) with no seepage have been superimposed on the data plot for a comparative study. It is apparent that, in general, the present data band lies above and below these curves for injection and suction, respectively. The only exception is the submerged wall jets data band with injection for $\tilde{x} > 1.2$, where the curve of the classical wall jet is higher. It is attributed to the fact that the classical wall jet is free from an overlying layer of reversed flow unlike the case of a submerged wall jet. However, the decay rate of jet velocity u_0, being influenced by the seepage, decreases in the presence of injection and increases with suction due to addition and extraction of momentum through the wall. The maximum departure of the average data trend with injection from the curve with no seepage is -11 % at $\tilde{x} = 1.2$ and that for suction is -17 % at $\tilde{x} = 0.6$.

The similarity characteristic of the individual u-profiles that exist in the fully developed zone of submerged wall jets is examined using the velocity scale u_0 and the vertical length scale y_1. In figure 13(*b*), the distributions of non-dimensional streamwise velocity u/u_0 are plotted against non-dimensional vertical distance $\tilde{y}(= y/y_1)$ for injection and suction. In general, the use of y_1 brings all the individual distributions of u onto a reasonably narrow band, justifying a similarity characteristic in the u-profiles in the presence of seepage flow through the wall. In the case of injection, the curve in the jet layer ($0 \leqslant \tilde{y} \leqslant 1$) has a distinct spatial lag (out of phase), shifting the point of maximum velocity ($u = u_0$) away from the wall, compared to curves of classical wall and submerged wall jets with no seepage. The inner-layer thickness [$0 \leqslant \tilde{y}(u/u_0 = 1)$] of individual distributions of u increases in the presence of injection, deflecting u away from the wall (figure 14*a*). This deflection of u from the curve of a submerged wall jet with no seepage is a maximum of -26 % at $\tilde{y} = 0.14$. However, the suction does not cause any significant spatial lag in the jet layer (figure 13*b*). Nevertheless, the near-wall data trend in the inner layer of the jet with suction has a small departure from the curves of classical wall and submerged wall jets with no seepage (figure 14*a*), because the extraction of momentum thickens the u-profiles (Mendoza & Zhou 1992). In the circulatory flow layer, the velocity data bands for both injection and suction lie just below the curve of the classical wall jet, where the entrainment of the reversed flow produces a consistent $u/u_0 < 1$. In figure 14(*b*), the velocity distributions in the inner layer of the jet are compared with the logarithmic law $u/u_\tau = \kappa^{-1}\ln(yu_\tau/\upsilon) + 5.5$, where κ is the von Kármán constant. The logarithmic law overestimates the velocity distributions in general. Wygnanski *et al.* (1992), who explored the applicability of different scaling laws of the turbulent wall jet, argued that the logarithmic law is not applicable to wall jets. Moreover, in the presence of injection and suction, the velocity distributions depart further from the logarithmic law. The thickening process of the jet layer is also evident in figure 14(*c*), which shows the horizontal variation of non-dimensional vertical length scale y_1/b. The half-width y_1 of a jet with injection increases faster than those of classical wall and submerged wall jets with no seepage. For $\hat{x} > 15$, the slope $\mathrm{d}y_1/\mathrm{d}x = 0.088$ for

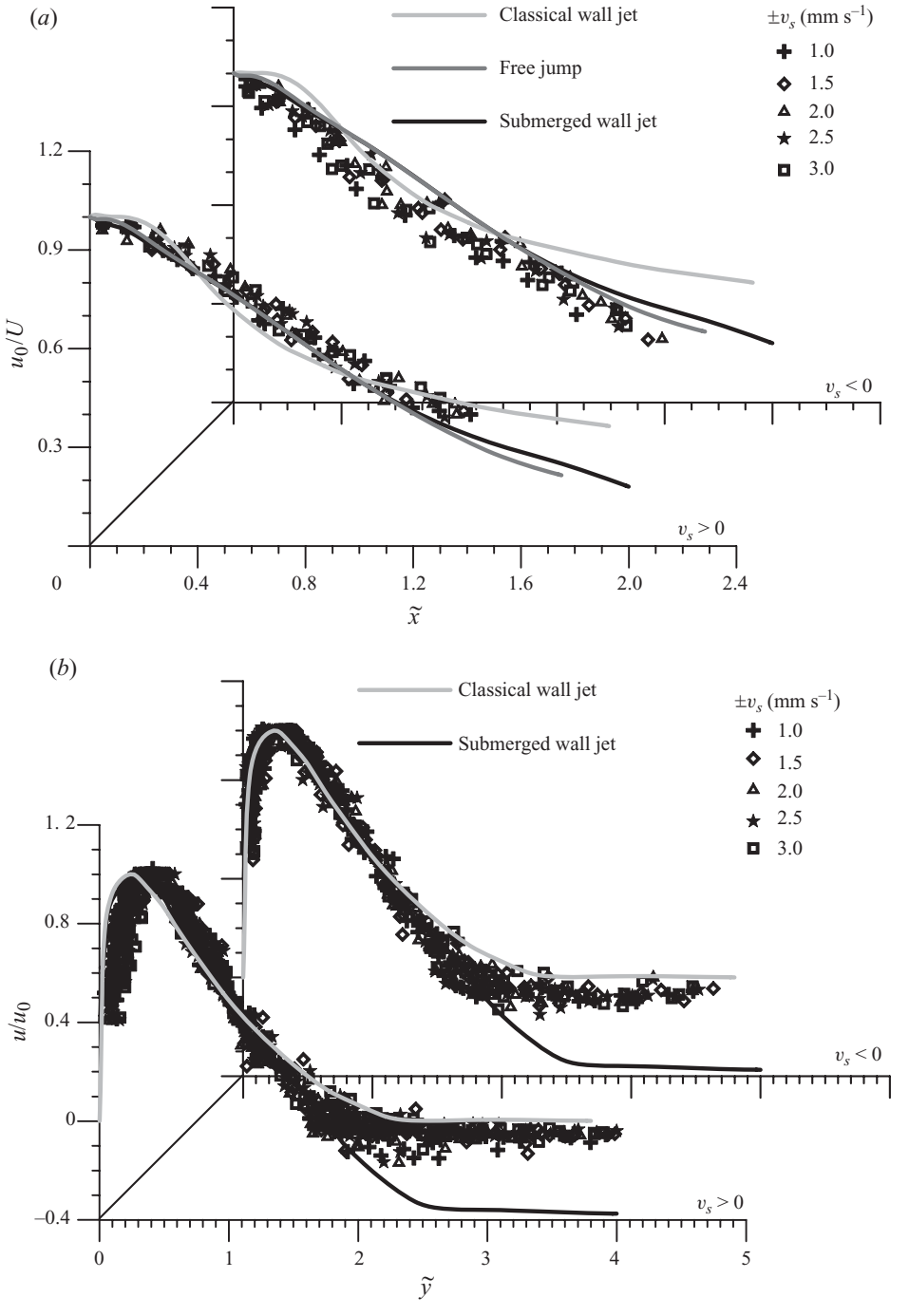

FIGURE 13. (*a*) u_0/U as a function of $\tilde{x}$ and (*b*) u/u_0 as a function of $\tilde{y}$ in submerged wall jets subjected to different v_s.

submerged wall jets subjected to injection is less than that for the classical wall jet ($\mathrm{d}y_1/\mathrm{d}x = 0.073$) (Launder & Rodi 1981). However, y_1 is not influenced by the suction (figure 14*c*).

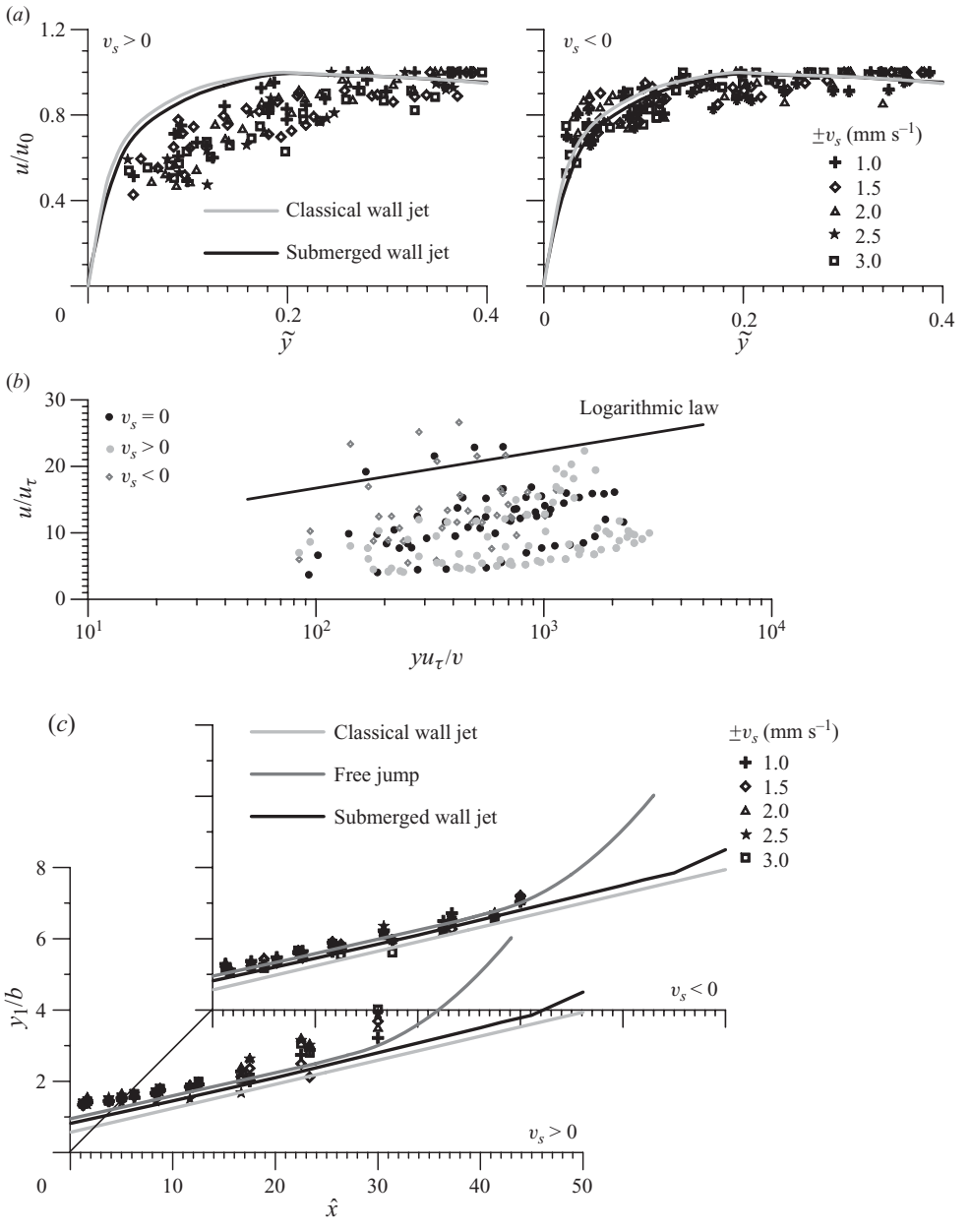

FIGURE 14. (*a*) u/u_0 as a function of $\tilde{y}$, (*b*) comparison of u/u_τ versus yu_τ/υ plots with logarithmic law and (*c*) variations of y_1/b with $\hat{x}$ in submerged wall jets subjected to different v_s.

5.3. *Similarity characteristics of Reynolds shear stress and turbulence intensities*

Figure 15(*a–c*) shows that the use of horizontal length scale λ could also bring all the data of $(uv^+)_0/(uv^+)_m$, $(u^+)_0/(u^+)_m$ and $(v^+)_0/(v^+)_m$ to collapse onto a narrow band, where the subscript '*m*' refers to a maximum for an experimental condition. It implies that there prevails a plausible similarity in the Reynolds shear stress and turbulence intensity distributions in submerged wall jets subjected to injection and

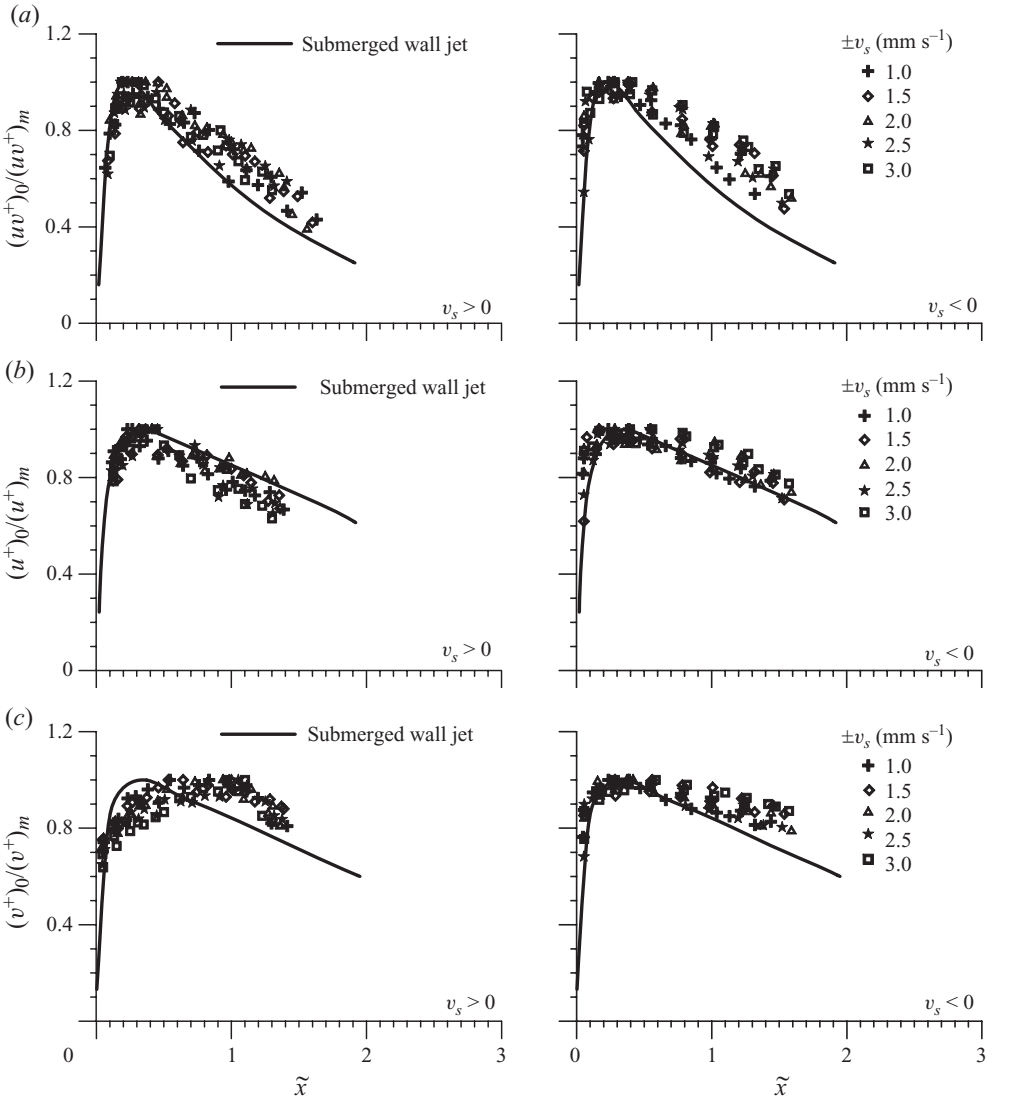

FIGURE 15. Dependence of (*a*) $(uv^+)_0/(uv^+)_m$ on $\tilde{x}$, (*b*) $(u^+)_0/(u^+)_m$ on $\tilde{x}$ and (*c*) $(v^+)_0/(v^+)_m$ on $\tilde{x}$ in submerged wall jets subjected to different v_s.

suction from the wall. However, some degree of scatter in the distributions remains because of the inherent dissemination of attenuating fluctuations in the turbulent flow. A comparison of the present data trends with the curves of a submerged wall jet with no seepage shows that the present trends have a spatial lag of the locations of their respective maxima from those of the submerged wall jet with no seepage due to the influence of seepage. The locations of $(uv^+)_m$, $(u^+)_m$ and $(v^+)_m$ with injection shift away from the origin and those with suction shift towards the jet origin from those of the submerged wall jet with no seepage. The maximum shift that is noticeable in the case of $(v^+)_m$ with injection from the location of $(v^+)_m$ with no seepage is $\tilde{x} = 1$. The curves also suggest that the decay rates of $(uv^+)_0$, $(u^+)_0$ and $(v^+)_0$ in submerged wall jets with seepage are slower than those with no seepage, as the injection and

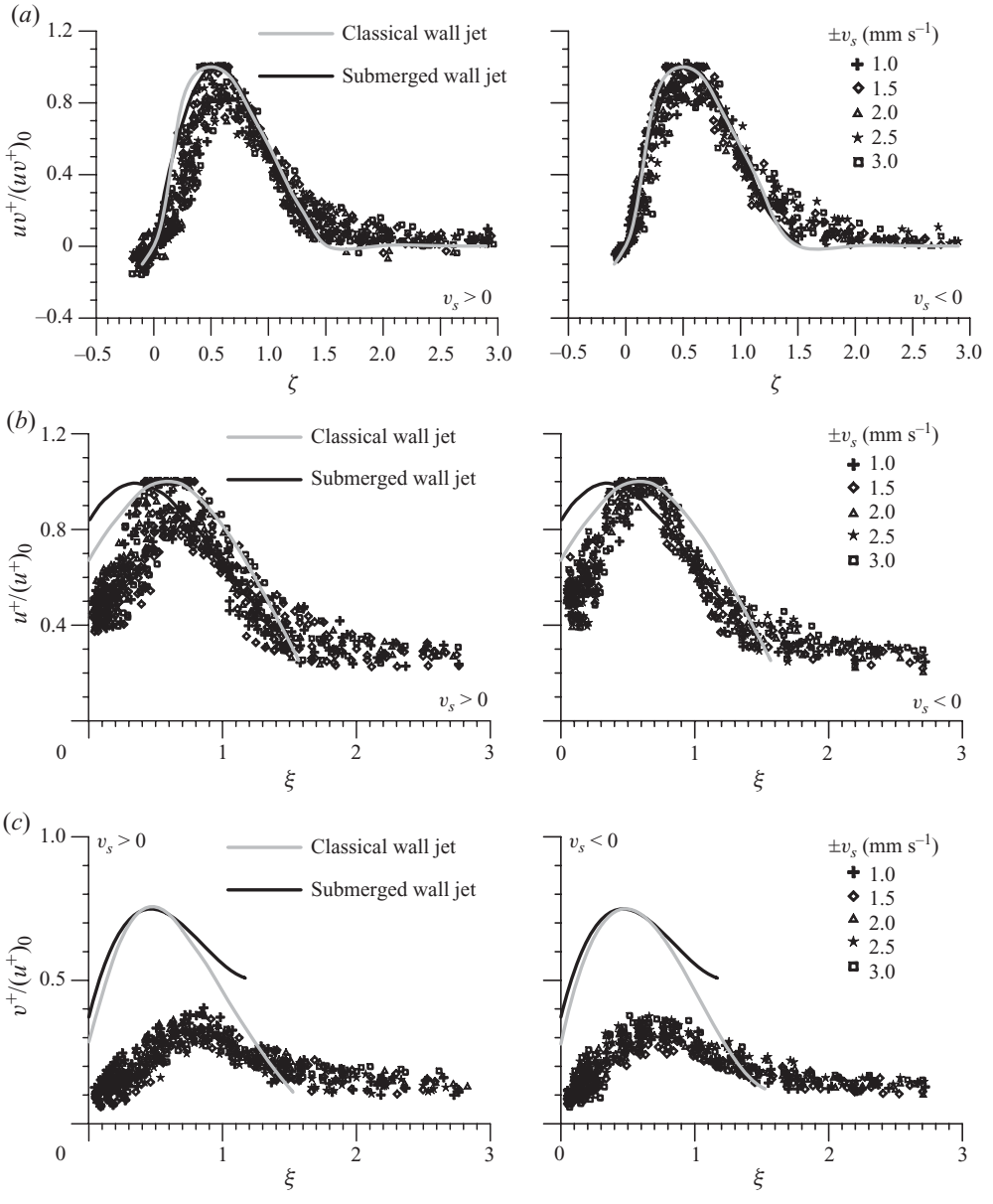

FIGURE 16. Similarities of distributions of (*a*) uv^+, (*b*) u^+ and (*c*) v^+ in submerged wall jets subjected to different v_s.

suction from the wall induce additional turbulence by mixing of fluid. For $(u^+)_0$ with injection, there is an exception, as the decay rate of $(u^+)_0$ becomes faster.

To examine the degree of similarity in the individual distributions of uv^+, u^+ and v^+, which exist in submerged wall jets subjected to injection and suction from the wall, the data of $uv^+/(uv^+)_0$ against $\zeta[= (y - \delta_1)/(y_2 - \delta_1)]$, $u^+/(u^+)_0$ against $\xi(= y/y_2)$ and $v^+/(u^+)_0$ against ξ are plotted in figure 16(*a–c*), respectively. The use of appropriate vertical length scales makes it possible to collapse the Reynolds shear stress and turbulence intensities data onto a relatively wide band. In this context,

note that it is a difficult proposition to achieve a slim band for the turbulence stresses because of inherent high attenuating turbulence fluctuations in the measurements. Nevertheless, the collapse achieved in these plots is reasonable for the confirmation of a similarity in the individual distributions of uv^+, u^+ and v^+. In figure 16(*a*), the inner-layer distributions of $uv^+/(uv^+)_0$ with injection lie above those of classical wall and submerged wall jets with no seepage. Also, in figure 16(*b*), a similar nature is apparent in the inner-layer distributions of $u^+/(u^+)_0$ with both injection and suction; but in figure 16(*a*), this nature is not prominent with suction. However, no spatial lag is apparent, as the maxima of the data bands appear on those of the curves of classical wall and submerged wall jets with no seepage. On the other hand, in figure 16(*c*), the mean trend of $v^+/(u^+)_0$ with seepage flow has a spatial lag from those of classical wall and submerged wall jets with no seepage, attaining maxima at $\xi = 0.9$ and 0.7 for injection and suction, respectively. To be more explicit, the seepage effect results in increasing the inner-layer thickness of v^+-profiles. The most noticeable features are that $u^+ = 0.4(u^+)_0$ in the beginning of the fully developed zone (figure 16*b*), which is in contrast to $0.8(u^+)_0$ in submerged wall jets with no seepage. On the other hand, $(v^+)_0$ is approximately $0.35(u^+)_0$ in the fully developed zone (figure 16*c*), which is also in contrast to $0.75(u^+)_0$ in submerged wall jets with no seepage (Long *et al.* 1990). This high value of $(v^+)_0 = 0.75(u^+)_0$ in submerged wall jets with no seepage invites uncertainties, as in open-channel flows, v^+/u^+ is on the order of 0.55 (Nezu & Nakagawa 1993). Only a strong wake flow can increase this ratio up to 0.7 (Townsend 1976). Reverting to the discussion of figure 16(*c*), the alteration in the distribution patterns of Reynolds shear stress and turbulence intensities is therefore influenced by the change of the inner-layer turbulence level in the presence of seepage having a significant diminishing magnitude of v^+ (about 40 %).

Figure 17(*a*, *b*) shows the variations of y_2/b with $\hat{x}$. It suggests the decay of half-width of $-\overline{u'v'}$ with the horizontal distance under seepage. The non-dimensional half-width y_2/b with injection and suction remains invariant with that of a submerged wall jet with no seepage. In figure 17(*b*), the variations of non-dimensional elevation of the null point δ_1/b of $-\overline{u'v'}$ with $\hat{x}$ are presented. The values of δ_1/b with injection are higher (by an average of 40 %) than those of the submerged wall jet with no seepage, whereas suction does not cause any change of δ_1/b from those of a submerged wall jet with no seepage.

6. Third-order moments of velocity fluctuations, turbulent kinetic energy and energy budget

6.1. *Third-order moments*

Notwithstanding several studies on the time-averaged flow characteristics, there remains little universal conformity in the characteristics of the mean third-order moments of velocity fluctuations (Keirsbulck *et al.* 2001). The knowledge of the third-order moments remains inadequate, especially on submerged wall jets in general and those subjected to seepage through the wall in particular. Third-order moments that contain important stochastic information relating to the flux of the stresses developed because of turbulence are directly attributable to the coherent structures (Gad-el-Hak & Bandyopadhyay 1994). To be more explicit, third-order moments preserve their sign, positive or negative, providing useful stochastic information on the temporal distribution of the velocity fluctuations with respect to the time-averaged velocity.

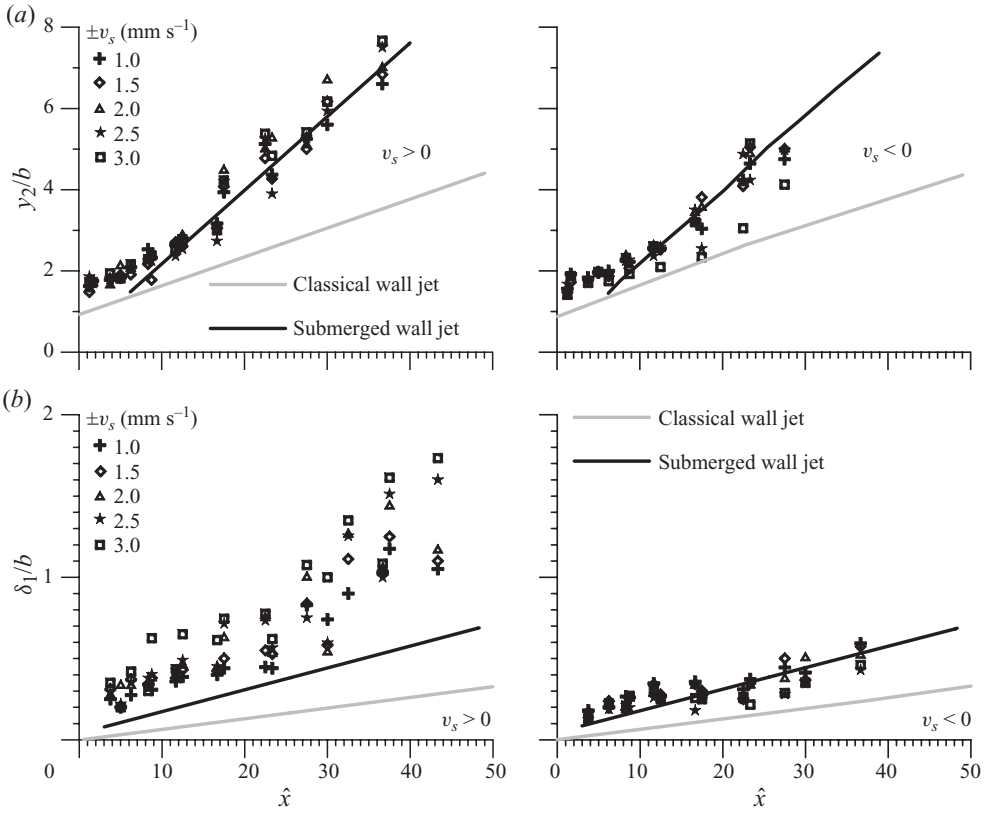

FIGURE 17. Variations of (*a*) y_2/b with $\hat{x}$ and (*b*) δ_1/b with $\hat{x}$ in submerged wall jets subjected to different v_s.

The set of third-order moments can be specified as follows (Raupach 1981):

$$M_{jk} = \overline{\tilde{u}^j \tilde{v}^k}, \tag{6.1}$$

where $\tilde{u} = u'/(\overline{u'u'})^{0.5}$ and $\tilde{v} = v'/(\overline{v'v'})^{0.5}$. In (6.1), $j + k = 3$, so that M_{30} and M_{03} are the 'skewness' of u' and v', respectively. Figure 18(*a–d*) suggests that in the fully developed zone of submerged wall jets, the third-order moments follow reasonably universal distributions whose near-wall portion is slightly changed by the seepage flow. The distribution patterns of all M_{jk} within the jet layer are quite similar and closely correlated with each other. Nonetheless, these third-order moments describe the general turbulence behavioural structure of submerged wall jets.

In figure 18(*a*), the skewness of u', $M_{30}[= \overline{\tilde{u}^3} = \overline{u'u'u'}/(\overline{u'u'})^{1.5}]$ describes the asymmetry in the distribution of the probability density of u'. From the viewpoint of hydrodynamics, M_{30} can be interpreted as the streamwise flux of the Reynolds normal stress $\overline{u'u'}$. Within the inner layer of the jet, M_{30} plots start with small negative values (that is close to zero) near the wall, reaching negative peaks (average value of $M_{30} \approx -1.3$) at the point of maximum jet velocity (approximately at $Y = 0.05$, where $Y = y/h$). Within $0.17 \leqslant Y \leqslant 0.25$, the changeover and the positive peaks (average value of $M_{30} \approx 1.2$) of M_{30} occur at the point of maximum Reynolds shear stress $-\overline{u'v'}$ and on the separation line (that is near the inflection point of the $-\overline{u'v'}$-profile), respectively. With further increase in Y, the M_{30} data band moves towards the vertical axis ($M_{30} = 0$) decreasing further to small negative values (average value

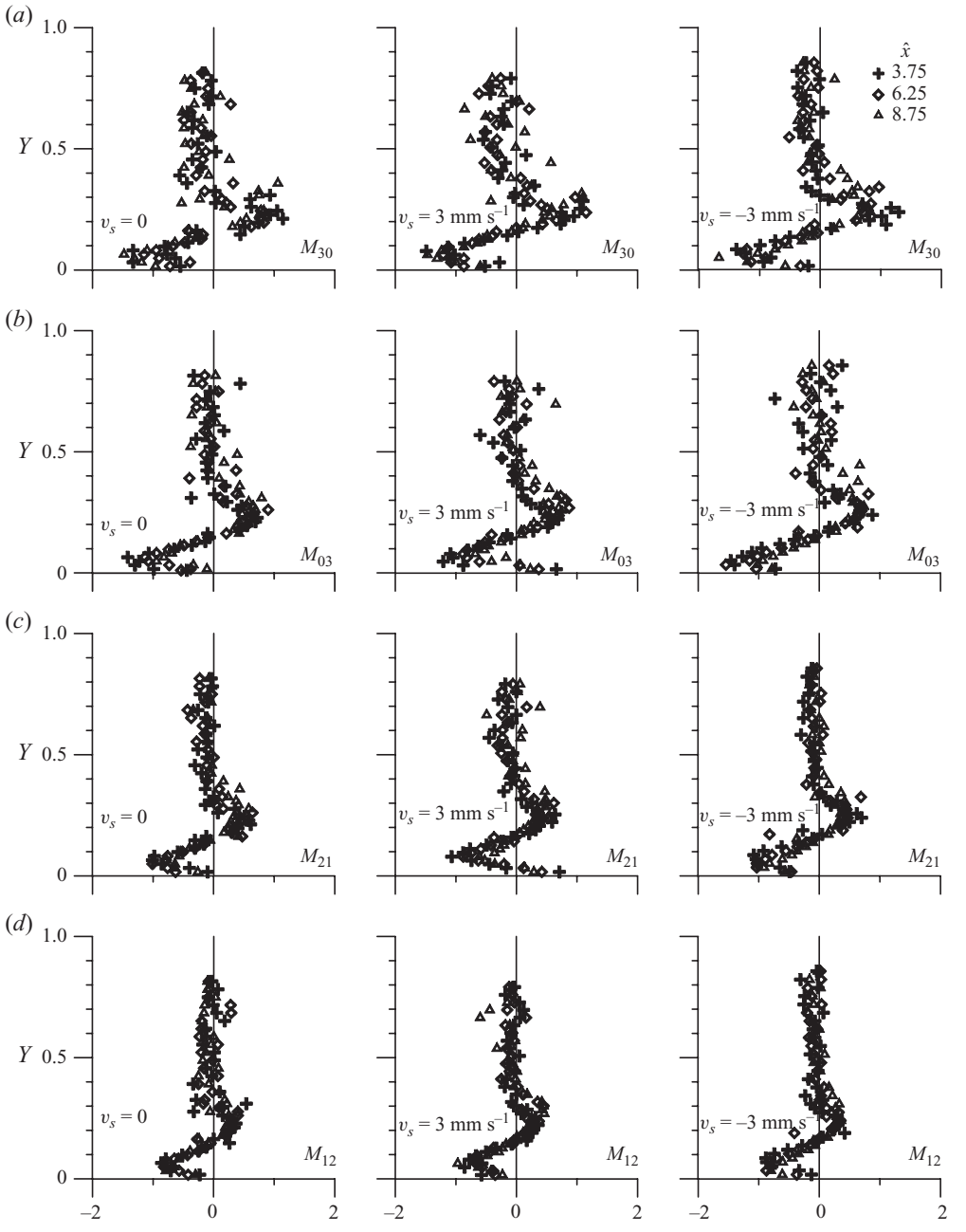

FIGURE 18. Distributions of third-order moments of u' and v' in submerged wall jets subjected to different v_s: (*a*) $M_{30}(Y)$, (*b*) $M_{21}(Y)$, (*c*) $M_{12}(Y)$ and (*d*) $M_{03}(Y)$.

of $M_{30} \approx -0.15$) and remaining almost constant along Y in the reversed flow layer. There exists an intense mixing because of momentum exchange resulting in a Gaussian distribution of u' having a skewness tending to near-zero values. Negative values of M_{30} near the wall (in the inner layer of the jet) indicate that the data are skewed left (that is the left tail is longer than the right tail) in the distribution of probability density of u'. On the other hand, near the inflection point of the $-\overline{u'v'}$-profile, the

positive values indicate that the data are skewed right. In this context, it is important to mention that the negative and positive values of M_{30} also suggest that the $\overline{u'u'}$-flux travels towards the jet origin and in the streamwise direction, respectively. In the reversed flow layer, the distributions of M_{30} remain with low negative values because of the arrival of low-speed fluid streaks from the upper flow zone. Besides M_{30}, other third-order moments are $M_{21} = \overline{u'u'v'}/[(\overline{u'u'})^{0.5}]$ that defines the turbulent advection of $\overline{u'u'}$ in the y-direction, $M_{12} = \overline{u'v'v'}/[(\overline{u'u'})^{0.5}(\overline{v'v'})]$ that refers to the turbulent advection of $\overline{v'v'}$ in the x-direction and $M_{03}[= \overline{v'v'v'}/[(\overline{v'v'})^{1.5}]$ that describes the vertical flux of the Reynolds normal stress $\overline{v'v'}$. The distributional variations of $M_{21}(Y)$, $M_{12}(Y)$ and $M_{03}(Y)$ plotted in figure 18(*b–d*) are quite similar to those of M_{30}. All third-order moments are close to zero near the wall. The virtual responses of burst events to the Reynolds shear stress production at a point can reasonably be ascertained by the third-order moments of the velocity fluctuations (Nakagawa & Nezu 1977). Within the inner layer of the jet, the negative peak values of M_{30} being larger than M_{21} and those of M_{03} larger than M_{12} indicate downward low-speed fluid streaks, inducing a strong retardation in the jet. However, within the outer layer of the jet, the positive peak values of M_{30} being larger than M_{21} and those of M_{03} larger than M_{12} indicate upward high-speed fluid streaks, inducing a strong acceleration in the jet. This phenomenon has an interpretation in terms of bursting events as the arrival of high-speed fluid streaks from the outer layer is associated with the outward interactions. In contrast, in the inner layer of the jet, the arrival of low-speed fluid streaks resulting from wall resistance is associated with inward interactions. The crossover point (that is the occurrence of the change of sign) in the skewness profile is related to the changeover from low- to high-speed fluid streaks. The above discussion has so far been made on general turbulence characteristics of submerged wall jets. However, the influence of injection and suction on third-order moments is apparent in the near-wall flow of the inner layer. The near-wall data of M_{21} and M_{03} become positive in submerged wall jets subjected to injection, indicating ejections in the form of entrainment of low-speed fluid streaks (as M_{12} and M_{30} remain negative) due to an addition of slow momentum through the wall. A close examination of the distributions of M_{21} and M_{03} corroborates that the signature of suction remains in the near-wall data of M_{21} and M_{03}. They have greater negative values than those with no seepage, suggesting an inward interaction due to an extraction of momentum through the wall. Although the representation of the third-order moments is useful, some information might remain implicit because of the averaging process associated with parameters involved. Therefore, to further enhance the illustration of the Reynolds shear stress production in the submerged wall jets, a quadrant analysis is carried out in § 7.

6.2. *Turbulent kinetic energy and energy budget*

The streamwise and vertical fluxes of the turbulent kinetic energy are expressed by $f_{ku} = 0.75(\overline{u'u'u'} + \overline{u'v'v'})$ and $f_{kv} = 0.75(\overline{v'v'v'} + \overline{v'u'u'})$, respectively (Raupach 1981; Krogstad & Antonia 1999; Bey, Faruque & Balachandar 2007). The vertical distributions of streamwise and vertical fluxes of the non-dimensional turbulent kinetic energy $F_{ku}(= f_{ku}/U^3)$ and $F_{kv}(= f_{kv}/U^3)$ at different $\hat{x}$ in submerged wall jets subjected to different v_s are presented in figure 19(*a–c*). Importantly, turbulent energy is generated in excess of dissipation, and the dissipation rate is higher in an energy-deficient zone. Therefore, the energy is transported from the energy-rich to the energy-deficient zone through a transition zone establishing a kinematic equilibrium. The negative magnitude of streamwise flux F_{ku} in the near-wall zone suggests that

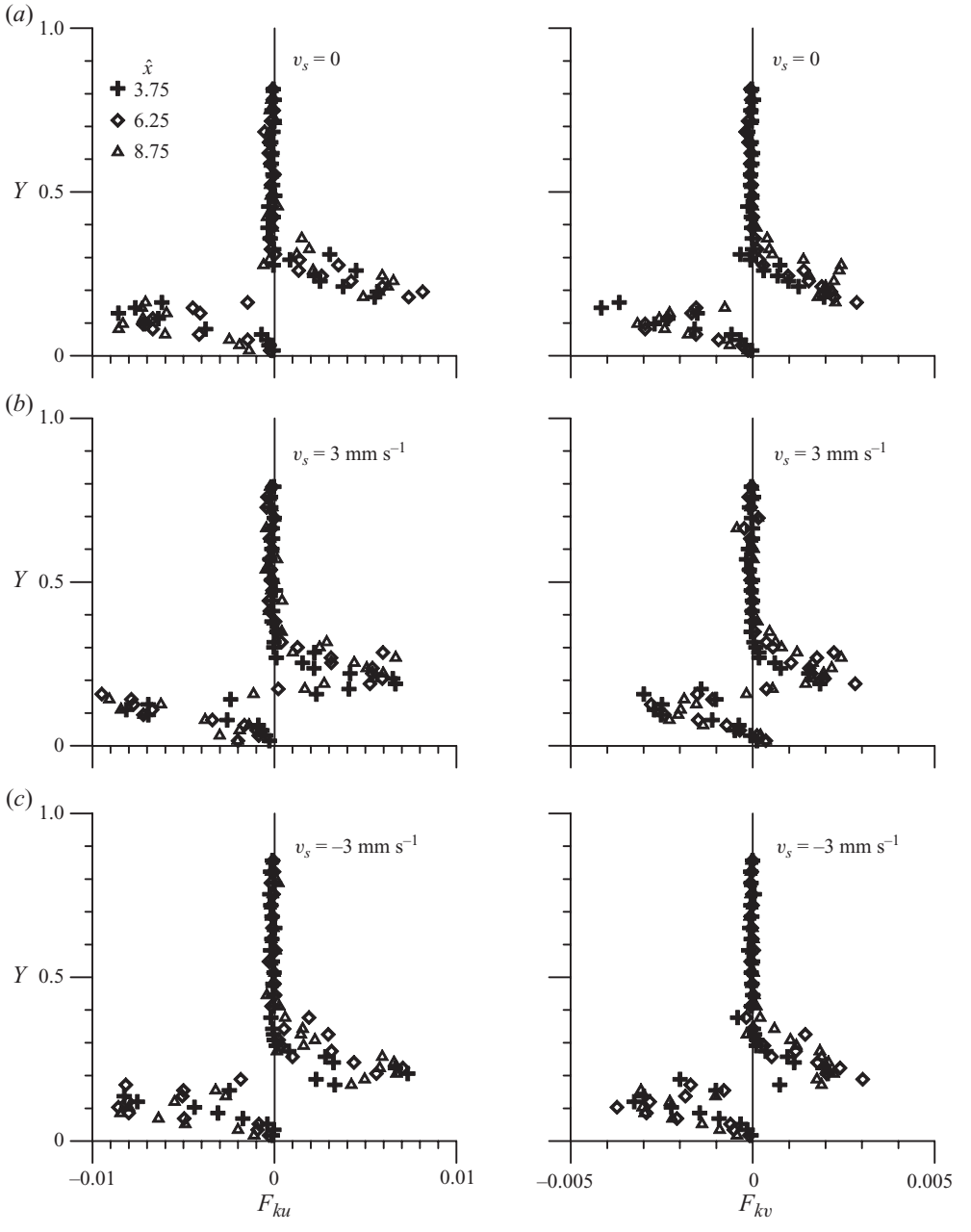

FIGURE 19. Distributions of the streamwise and vertical fluxes of turbulent kinetic energy in submerged wall jets subjected to (*a*) $v_s = 0$, (*b*) $v_s = 3\,\mathrm{mm\,s^{-1}}$ and (*c*) $v_s = -3\,\mathrm{mm\,s^{-1}}$.

the transport is directed towards the jet origin. The peak value of F_{ku} in the near-wall zone is located below the point of maximum $-\overline{u'v'}$ coinciding with the peak of M_{21}. The advection terms are therefore pertinent in the energy transport mechanism. With increasing Y, F_{ku} changes sign. The point of crossover occurs at the point of maximum $-\overline{u'v'}$, and then the transport is streamwise reaching a positive peak near the inflection point of the $-\overline{u'v'}$-profile. With further increase in Y, F_{ku} drops

down drastically, becoming negligible in the reversed flow layer. It is obvious that within the jet layer, the streamwise energy flux is negative transporting towards the jet origin. To be more explicit, within the jet layer, the inertia of fluid streaks induces a resilience effect resulting in negative F_{ku}. On the other hand, the negative magnitude of the vertical flux F_{kv} in the near-wall zone indicates a downward transport. The negative values of both F_{ku} and F_{kv} imply that the turbulent kinetic energy flux transports towards the jet origin and, at the same time, the inward interactions prevail. The distributions of F_{kv} follow a similar distribution pattern to F_{ku} with a reduced magnitude. It also suggests that above the inflection point of the $-\overline{u'v'}$-profile, outward interactions are the dominant mechanism. The influence of seepage is only noticeable in the near-wall plots of F_{kv} with injection. The positive values of F_{kv} and the corresponding negative values of F_{ku} imply a weak ejection induced by the injection from the wall.

The turbulent energy budget in a two-dimensional shear flow is defined by the turbulent production $t_P[=-\overline{u'v'}(\partial u/\partial y)]$ that is balanced by the turbulent dissipation ε, turbulent energy diffusion $t_D(=\partial f_{kv}/\partial y)$, pressure energy diffusion $p_D[=(\overline{p'v'/\rho})/\partial y]$ and viscous diffusion $v_D[=-\upsilon(\partial^2 k/\partial y^2)]$, where p' is the pressure fluctuation and k is the turbulent kinetic energy (Nezu & Nakagawa 1993). Importantly, viscous diffusion v_D is negligible in flows having high Reynolds numbers. The turbulent dissipation ε is estimated using the following relationship (Irwin 1973; Krogstad & Antonia 1999):

$$\varepsilon = \frac{15\upsilon}{u^2}\overline{\left(\frac{\partial u'}{\partial t}\right)^2}. \tag{6.2}$$

The pressure energy diffusion p_D is determined as the residual of the equation of the turbulent energy budget as $p_D = t_P - \varepsilon - t_D$. Figure 20(*a–c*) shows the turbulent energy budget, measured at $\hat{x} = 6.25$, in submerged wall jets subjected to $v_s = 0$, 3 and $-3\,\mathrm{mm\,s^{-1}}$. The symbols T_P, E_D, T_D and P_D represent non-dimensional forms of t_P, ε, t_D and p_D, respectively, by using a factor h/U^3. In figure 20(*a–c*), T_P increases rapidly with an increase in Y from the wall attaining a peak at the point of maximum $-\overline{u'v'}$, and then it decreases rapidly becoming nearly constant (having a small magnitude) in the reversed flow layer. Positive values of T_P represent the transformation of energy from time-averaged flow to turbulence, while the reverse transformation is true for negative values of T_P. The distributions of E_D are similar to those of T_P with a spatial lag of approximately $0.05Y$. Consequently, the peak of T_P occurs at the inflection point of the $-\overline{u'v'}$-profile. Note that in open-channel flows, T_P becomes nearly equal to E_D (having a small lag) (Nezu & Nakagawa 1993). On the other hand, the distributions of T_D and P_D are opposing in nature, and thus they balance each other. The negative peak of T_D and the positive peak of P_D correspond to the point of maximum $-\overline{u'v'}$, while the positive peak of T_D and the negative peak P_D take place at the inflection point of the $-\overline{u'v'}$-profile. Importantly, negative values of T_D and P_D represent a gain in turbulent production. Here, the occurrence of a null point of $-\overline{u'v'}$ below the point of maximum u can be explained (see figures 3 and 8). At the point of maximum u, $-\overline{u'v'}$ is negative, and figure 20 indicates that the turbulent energy diffusion of negative $-\overline{u'v'}$ towards the maximum u from the outer layer dominates that of positive $-\overline{u'v'}$ from the inner layer.

7. Quadrant analysis

To quantify the total Reynolds shear stress $-\overline{u'v'}$ at a specific point as a sum of contributions from different bursting events, it is a traditional approach to arrange the

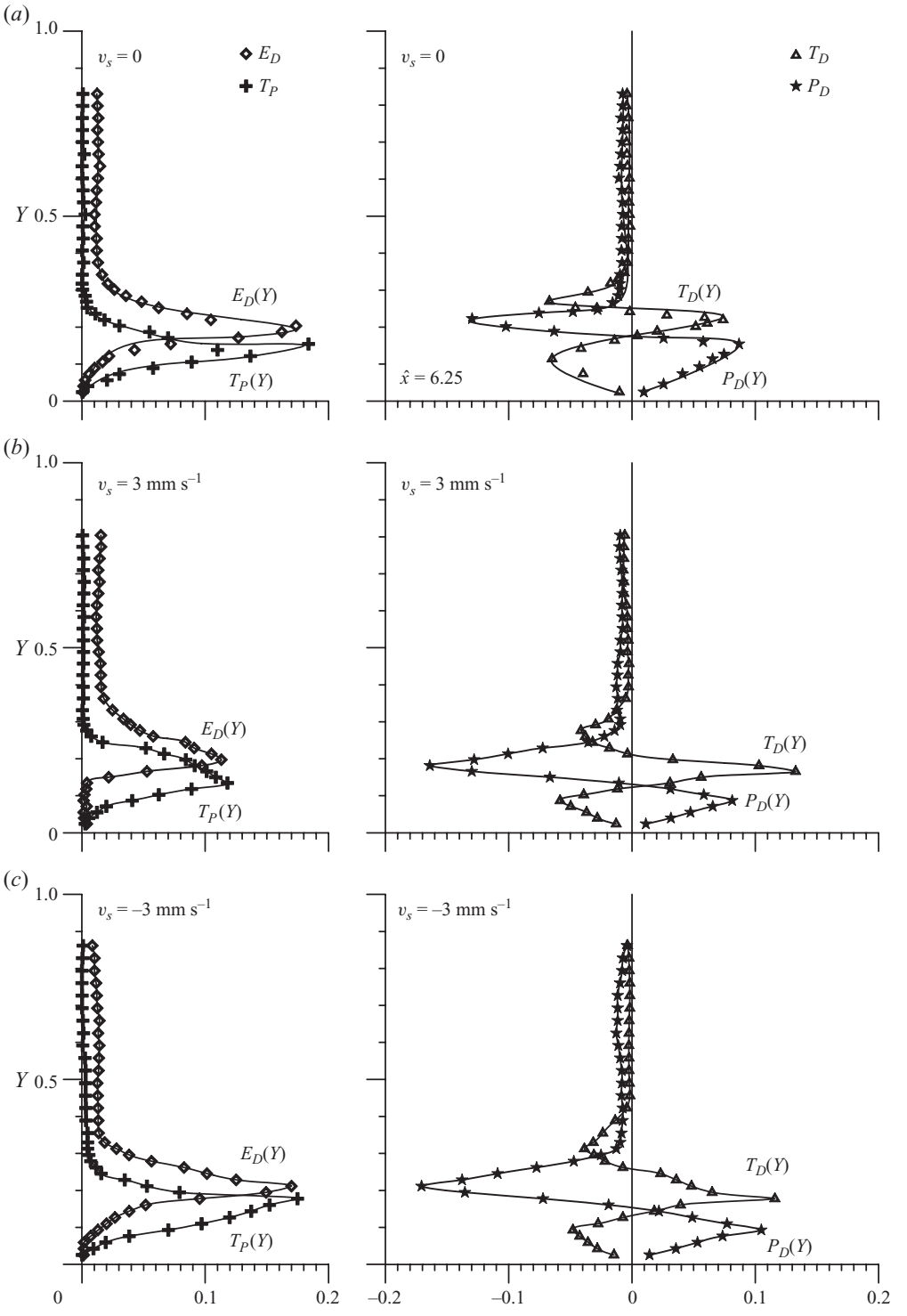

FIGURE 20. Turbulent energy budget in submerged wall jets subjected to (*a*) $v_s = 0$, (*b*) $v_s = 3\,\mathrm{mm\,s^{-1}}$ and (*c*) $v_s = -3\,\mathrm{mm\,s^{-1}}$.

components of velocity fluctuations (u' and v') according to quadrant on the $u'v'$-plane (Lu & Willmarth 1973). Introducing a parameter H called 'hole size' that represents threshold level as explained by Nezu & Nakagawa (1993), the size of the hole is decided by the curve $|u'v'| = H(\overline{u'u'})^{0.5}(\overline{v'v'})^{0.5}$. With this method, large contributions to $-\overline{u'v'}$ from each quadrant can be extracted leaving the smaller velocity fluctuations (u' and v') that belong to the hole corresponding to more quiescent periods. Therefore, the hole size H allows differentiation between strong and weak events for small values of H and only strong events for large values of H. Let the four quadrants ($i = 1$, 2, 3 and 4) refer to the bursting events, which are outward interactions ($i = 1; u' > 0, v' > 0$), ejections ($i = 2; u' < 0, v' > 0$), inward interactions ($i = 3; u' < 0, v' < 0$) and sweeps ($i = 4; u' > 0, v' < 0$). The conditional stochastic analysis can be performed introducing a detection function $\lambda_{i,H}(t)$ defined by

$$\lambda_{i,H}(y,t) = \begin{cases} 1, & \text{if } (u',\ v') \text{ is in quadrant } i \text{ and if } |u'v'| \geqslant H(\overline{u'u'})^{0.5}(\overline{v'v'})^{0.5}, \\ 0, & \text{otherwise.} \end{cases} \tag{7.1}$$

At any point, the contribution to the total Reynolds shear stress production from the quadrant i outside the hole of size H is given by

$$\langle u'v' \rangle_{i,H} = \lim_{T\to\infty} \frac{1}{T} \int_0^T u'(t)v'(t)\lambda_{i,H}(y,t)\,\mathrm{d}t. \tag{7.2}$$

The Reynolds shear stress fractional contribution $S_{i,H}$ to each event is

$$S_{i,H} = \frac{\langle u'v' \rangle_{i,H}}{\overline{u'v'}}. \tag{7.3}$$

To quantify the fractional contributions of the Reynolds shear stress from different bursting events in submerged wall jets subjected to no seepage, injection and suction, $S_{i,H}(Y)$ are plotted in figures 21(*a–c*) and 22(*a–c*) for the hole sizes $H = 0$ and 2, respectively. The high-frequency events ($H = 0$) associated with the use of all the data are important in a wall jet flow. In addition, the stronger events eliminating the weaker ones are obtained by fixing the hole size $H = 2$, which corresponds to the events that have greater Reynolds shear stress values, as most of the earlier studies have used this value of H (Balachandra & Bhuiyan 2007). The general contributions from the outward and inward interactions ($S_{1,0}$ and $S_{3,0}$) are most positive, and those from the ejections and sweeps ($S_{2,0}$ and $S_{4,0}$) are most negative having a change of sign of the near-wall data due to crossover of $-\overline{u'v'}$-profiles immediately above the wall (see figure 8*d*).

In figure 21(*a*), the inward interactions $S_{3,0}$ get stronger with Y becoming strongest at the point of maximum u (that is above the point of $-\overline{u'v'} = 0$), but this characteristic progressively disappears with an increase in $\hat{x}$ (that is with the decay of u_0). On the other hand, the outward interactions $S_{1,0}$ that are weakest near the wall get gradually stronger with Y, and maximum $S_{1,0}$, which represents a fast outward motion of fluid streaks from the wall jet, occurs at the inflection point of the $-\overline{u'v'}$-profile (that is on the separation line). In the inner layer of the jet, the smaller contribution from $S_{1,0}$ is accompanied by a greater contribution from $S_{3,0}$, indicating a decelerating process. Note that both the events $S_{1,0}$ and $S_{3,0}$ intersect at the point of maximum $-\overline{u'v'}$. However, this suggests that there exists a correlation between fast outward motion and slow entrainment of fluid streaks within the jet layer. Importantly, ejection and sweep events, which appear together, contribute little within the jet layer, although they contribute moderately within the reversed flow layer. It implies that the effect

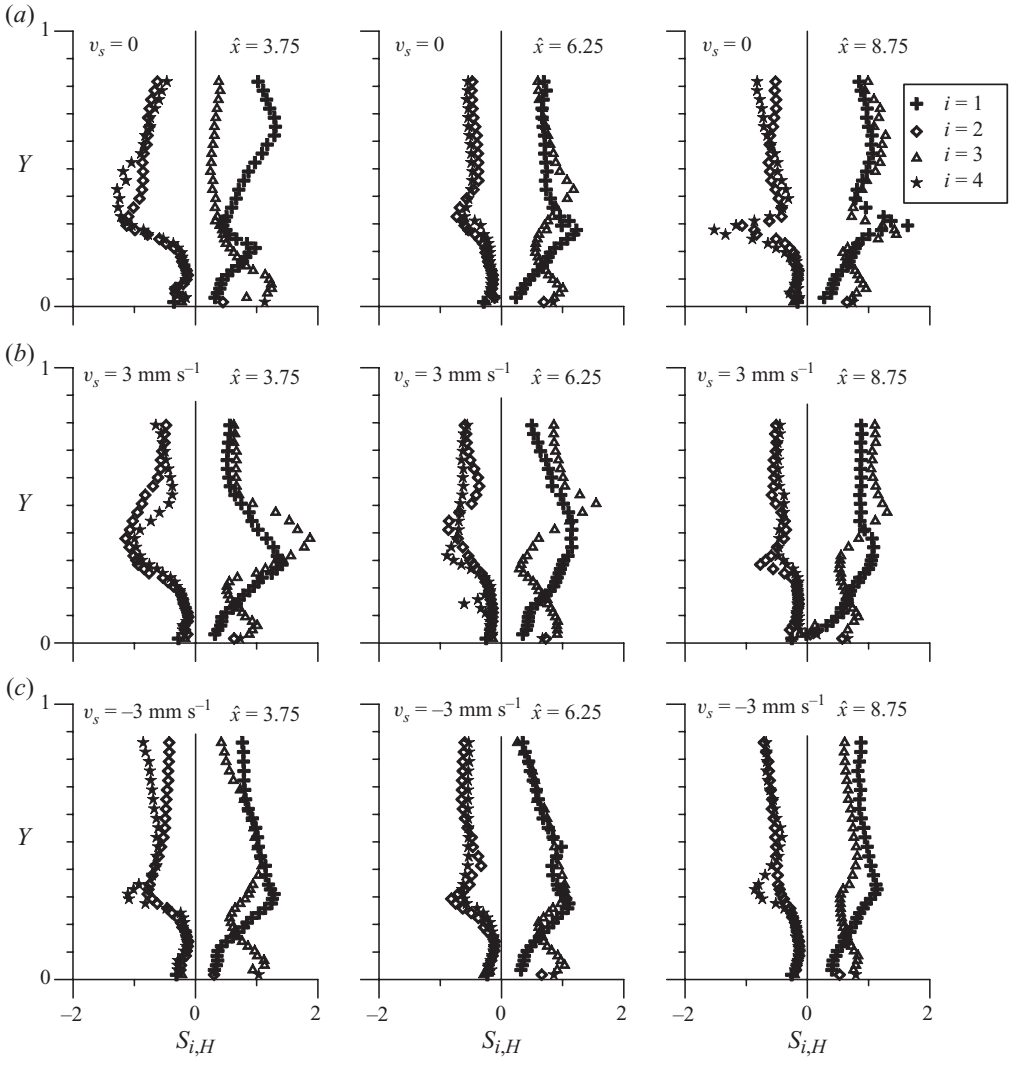

FIGURE 21. Variations of $S_{i,H}(Y)$ for $H = 0$ in submerged wall jets subjected to (*a*) $v_s = 0$, (*b*) $v_s = 3\,\mathrm{mm\,s^{-1}}$ and (*c*) $v_s = -3\,\mathrm{mm\,s^{-1}}$.

of ejection and sweep events cancel each other. In general, in the reversed flow layer, the contributions $S_{i,0}$ from different events become almost constant over Y for $\hat{x} > 3.75$. In figure 20(*b*), it is however noticeable that the contribution from the inward interactions $S_{3,0}$ is diminished in the presence of injection within the inner layer. Also, a close examination of the trend of ejection events $S_{2,0}$ in the case of injection suggests that there is an enhancement of $S_{2,0}$ with positive values in the immediate vicinity of the wall. This is in conformity with the results in figure 18(*b*, *d*). In figure 20(*b*), suction appears to influence $S_{i,0}$ data on the separation line.

Compared with the Reynolds shear stress contributions from more extreme events occurring for hole size $H = 2$ given in figure 22(*a–c*), the most energetic outward and inward interactions ($S_{1,2}$ and $S_{3,2}$) have distinct correlation across the flow depth, because a decrease in $S_{1,2}$ contributions is accompanied by an increase in $S_{3,2}$ contributions. However, there remains a general consensus in figures 21(*a–c*) and

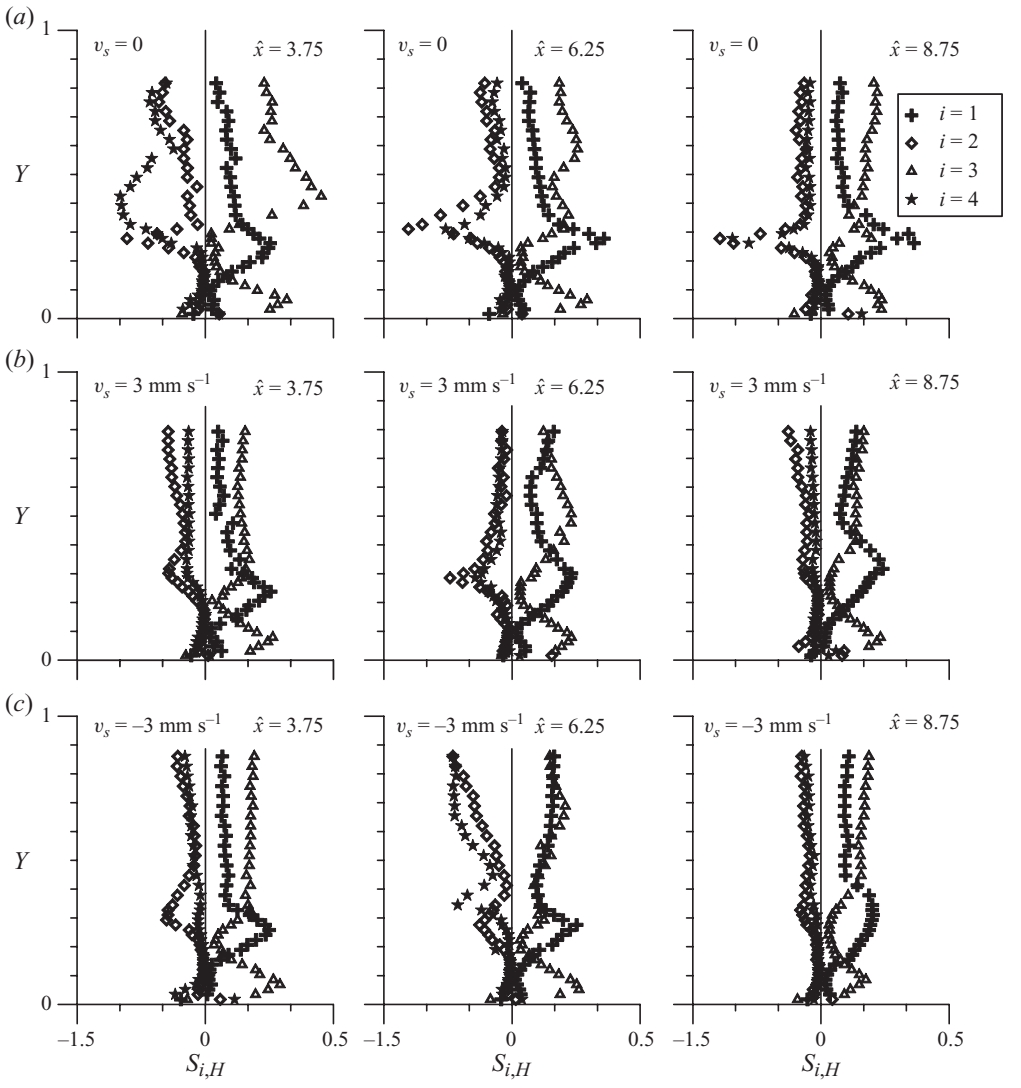

FIGURE 22. Variations of $S_{i,H}(Y)$ for $H = 2$ in submerged wall jets subjected to (*a*) $v_s = 0$, (*b*) $v_s = 3\,\mathrm{mm\,s^{-1}}$ and (*c*) $v_s = -3\,\mathrm{mm\,s^{-1}}$.

22(*a–c*) that the same nature of outward and inward interactions is prevalent within the jet layer. The contributions from the ejection $S_{2,2}$ and sweep $S_{4,2}$ events become relatively insignificant in this layer.

8. Concluding remarks

The vertical distributions of the time-averaged streamwise velocity component and the flow vectors exhibit a generalized depiction of the decay of the jet velocity in submerged wall jets subjected to injection and suction from the wall (figures 3 and 5). The rate of decay of jet velocity over the horizontal distance increases in the presence of injection and decreases with suction. Within the jet layer, the upward motion of the time-averaged vertical velocity component in the fully developed zone increases in the

presence of injection and decreases with suction because of addition and extraction of momentum in accordance with the mode of seepage flows through the wall (figure 4). As the jet layer is overlain by the circulatory flow layer in the developing zone, it gives rise to an increased turbulence level at the junction of these two layers, resulting in protuberances in the distributions of turbulence intensities and Reynolds shear stress at the top of the jet layer (figures 6–8). The magnitude of the protuberances in the distributions of streamwise turbulence intensity increases in the presence of injection and decreases with suction (figure 6). The height of the null point in the distributions of Reynolds shear stress in submerged wall jets with injection is greater than that with no seepage (figure 8). Also, the wall shear stress increases in the presence of injection and decreases with suction (figure 9). Based on the two-dimensional RANS equations of a steady turbulent flow, the time-averaged streamwise velocity and Reynolds shear stress distributions in the fully developed zone of submerged wall jets subjected to no seepage, injection and suction are computed (figures 10 and 11). The unknown constants in the developed equations of velocity and Reynolds shear stress are determined by calibrating the equations with the experimental data, treating certain constants as free parameters.

The turbulent flow characteristics of submerged wall jets subjected to injection and suction from the wall have been analysed from the viewpoint of the similarity characteristics, growth of the length scale and decay of the velocity and turbulence characteristics scales. The use of a horizontal length scale, which is the distance from the sluice opening to the location of the maximum jet velocity that equals half of the issuing jet velocity, brings all the data plots of velocity, Reynolds shear stress and turbulence intensities to collapse on a single band for the individual parameters (figures 13*a* and 15*a–c*). On the other hand, the vertical length scales are the half-width of the jet for the streamwise velocity distributions, the half-width of the Reynolds shear stress above the null point for the Reynolds shear stress distributions and the half-width of the Reynolds shear stress for the turbulence intensities. They enable the collapse of the data plots of individual distributions of streamwise velocity, Reynolds shear stress and turbulence intensities onto a narrow band (figures 13*b* and 16*a–c*). It implies that the streamwise velocity, Reynolds shear stress and turbulence intensities in the fully developed zone are reasonably similar under both injection and suction. The decay rate of the local maximum jet velocity is slower in the presence of injection and faster with suction (figure 13*a*). On the other hand, the decay rate of the Reynolds shear stress and turbulence intensities is slower with both injection and suction than that with no seepage (figure 15*a–c*). The inner-layer thickness of individual velocity distributions increases in response to the injection, but the suction causes a small change in the jet layer (figure 14*a*). The inner-layer distributions of Reynolds shear stress with injection lay above those of the classical wall and submerged wall jets with no seepage (figure 16*a*). Also, a similar characteristic is apparent in the inner-layer distributions of the streamwise turbulence intensity with both injection and suction (figure 16*b*, *c*). The half-width of the jet with injection increases faster than that with no seepage, but it remains almost invariant with suction (figure 14*c*). In contrast, the half-widths of the Reynolds shear stress with injection and suction remain invariant with no seepage (figure 17*a*). The elevations of the null point of Reynolds shear stress with injection occur at a higher level than those with no seepage, whereas suction does not change the position of the null point (figure 17*b*).

Third-order moments of velocity fluctuations specify that the inner layer of the jet is associated with the arrival of low-speed fluid streaks causing a retardation. On the contrary, the upper layer of the jet is associated with the arrival of high-speed

fluid streaks causing an acceleration. Injection and suction influence the near-wall distributions of third-order moments by increasing the upward and downward turbulent advection of the streamwise Reynolds normal stress, respectively. They influence the vertical turbulent flux of the vertical Reynolds normal stress in a similar way (figure 18).

Within the jet layer, the streamwise turbulent energy flux travels towards the jet origin, while in the inner layer of the circulatory flow, it travels in the streamwise direction (figure 19). The turbulent energy budget is maintained by the turbulent and pressure energy diffusions opposing each other and by the turbulent dissipation lagging the turbulent production (figure 20).

In the quadrant analysis of the velocity fluctuations, the inward and outward interactions are the primary contributions to the Reynolds shear stress production in the inner and outer layers of the jet, although injection induces feeble ejections in the vicinity of the wall (figures 21 and 22).

While the primary aim of the investigation is to explore the effect of wall seepage on the turbulence characteristics of submerged wall jets, the third-order moments, turbulent energy and quadrant analyses help to discover the turbulence characteristics of these aspects in submerged wall jets on a smooth wall in general.

This is a part of the doctoral research work of T.K.N. under the supervision of S.D. funded by the QI programme. S.K.B. is grateful to the Centre for Theoretical Studies at the Indian Institute of Technology, Kharagpur, for providing fellowship to visit the Institute during the study.

REFERENCES

Amitay, M. & Cohen, J. 1993 The mean flow of a laminar wall jet subjected to blowing or suction. *Phys. Fluids* A **5**, 2053–2057.

Amitay, M. & Cohen, J. 1997 Instability of a two-dimensional plane wall jet subjected to blowing or suction. *J. Fluid Mech.* **344**, 67–94.

Balachandar, R. & Bhuiyan, F. 2007 Higher-order moments of velocity fluctuations in an open-channel flow with large bottom roughness. *J. Hydr. Engng ASCE* **133**, 77–87.

Barenblatt, G. I., Chorin, A. J. & Prostokishin, V. M. 2005 The turbulent wall jet: a triple-layered structure and incomplete similarity. *Proc. Natl Acad. Sci.* **102**, 8850–8853.

Bey, A., Faruque, M. A. A. & Balachandar, R. 2007 Two-dimensional scour hole problem: role of fluid structures. *J. Hydr. Engng ASCE* **133**, 414–430.

Bose, S. K. & Dey, S. 2007 Theory of free surface flow over rough seeping beds. *Proc. R. Soc. Lond.* A **463**, 369–383.

Dey, S. 2002 Secondary boundary layer and wall shear for fully developed flow in curved pipes. *Proc. R. Soc. Lond.* A **458**, 283–298.

Dey, S. & Sarkar, A. 2006 Response of velocity and turbulence in submerged wall jets to abrupt changes from smooth to rough beds and its application to scour downstream of an apron. *J. Fluid Mech.* **556**, 387–419.

Dey, S. & Sarkar, A. 2008 Characteristics of turbulent flow in submerged jumps on rough beds. *J. Engng Mech. ASCE* **134**, 49–59.

Gad-el-hak, M. & Bandyopadhyay, P. 1994 Reynolds number effects in wall-bound turbulent flow. *Appl. Mech. Rev.* **47**, 307–365.

Gartshore, I. S. 1965 The streamwise development of two-dimensional wall jets and other two-dimensional turbulent shear flows. PhD thesis, McGill University, Montreal, Canada.

Glauert, M. B. 1956 The wall jet. *J. Fluid Mech.* **1**, 625–643.

Irwin, H. P. A. H. 1973 Measurements in a self-preserving plane wall jet in a positive pressure gradient. *J. Fluid Mech.* **61**, 33–63.

Keirsbulck, L., Mazouz, A., Labraga, L. & Tournier, C. 2001 Influence of the surface roughness on the third-order moments of velocity fluctuations. *Exps. Fluids* **30**, 592–594.

Krogstad, P. A. & Antonia, R. A. 1999 Surface roughness effects in turbulent boundary layers. *Exps. Fluids* **27**, 450–460.

Launder, B. E. & Rodi, W. 1981 The turbulent wall jet. *Prog. Aerospace Sci.* **19**, 81–128.

Launder, B. E. & Rodi, W. 1983 The turbulent wall jet-measurement and modelling. *Annu. Rev. Fluid Mech.* **15**, 429–459.

Long, D., Steffler, P. M. & Rajaratnam, N. 1990 LDA study of flow structure in submerged hydraulic jump. *J. Hydr. Res.* **28**, 437–460.

Lu, S. S. & Willmarth, W. W. 1973 Measurements of the structures of the Reynolds stress in a turbulent boundary layer. *J. Fluid Mech.* **60**, 481–511.

Mccorquodale, J. A. 1986 Hydraulic jumps and internal flows. In *Encyclopedia of Fluid Mechanics* (ed. N. P. Cheremisinoff), chapter 8, vol. 2. Gulf Publishing.

Mendoza, C. & Zhou, D. 1992 Effects of porous bed on turbulent stream flow above bed. *J. Hydr. Engng ASCE* **118**, 1222–1240.

Nakagawa, H. & Nezu, I. 1977 Prediction of the contributions to the Reynolds stress from bursting events in open-channel flows. *J. Fluid Mech.* **80**, 99–128.

Narasimha, R., Narayan, K. Y. & Parthasarathy, S. P. 1973 Parametric analysis of turbulent wall jets in still air. *Aeronaut. J.* **77**, 355–359.

Nezu, I. & Nakagawa, H. 1993 *Turbulence in Open-Channel Flows*. Balkema.

Patel, R. P. & Newman, B. G. 1961 Self-preserving, two-dimensional turbulent jets and wall jets in a moving stream. *Rep.* Ae 5. Mech. Engng Res. Lab., McGill University, Canada.

Rajaratnam, N. 1965 The hydraulic jump as a wall jet. *J. Hydr. Div. ASCE* **91**, 107–132.

Rajaratnam, N. 1976 *Turbulent Jets*. Elsevier Science.

Raupach, M. R. 1981 Conditional statistics of Reynolds stress in rough-wall and smooth-wall turbulent boundary layers. *J. Fluid Mech.* **108**, 363–382.

Schlichting, H. 1979 *Boundary Layer Theory*. McGraw-Hill.

Schwarz, W. H. & Cosart, W. P. 1961 The two-dimensional turbulent wall jet. *J. Fluid Mech.* **10**, 481–495.

Tachie, M. F., Balachandar, R. & Bergstrom, D. J. 2004 Roughness effects on turbulent plane wall jets in an open channel. *Exps. Fluids* **37**, 281–292.

Townsend, A. A. 1956 The properties of equilibrium boundary layers. *J. Fluid Mech.* **1**, 561–573.

Townsend, A. A. 1976 *The Structure of Turbulent Shear Flow*. Cambridge University Press.

Wygnanski, I., Katz, Y. & Horev, E. 1992 On the applicability of various scaling laws to the turbulent wall jet. *J. Fluid Mech.* **234**, 669–690.

Yang, S. Q., Tan, S. K. & Lim, S. Y. 2004 Velocity distribution and dip-phenomenon in smooth uniform open channel flows. *J. Hydr. Engng ASCE* **130**, 1179–118.